6-15-2019

Zinc ferrite based gas sensors: A review

Kaidi Wu

Jianzhi Li

Chao Zhang

Zinc Ferrite Based Gas Sensors: A Review

Kaidi Wu[a], Jianzhi Li[b], Chao Zhang[a,*]

a. College of Mechanical Engineering, Yangzhou University, Yangzhou 225127, P.R. China
b. Department of Manufacturing and Industrial Engineering, The University of Texas Rio Grande Valley, Edinburg, TX 78539, USA

* Corresponding author
Tel/Fax: +86-514-87436008
Email: zhangc@yzu.edu.cn
zhangchao_cqu@hotmail.com

Abstract:

Flammable, explosive and toxic gases, such as hydrogen, hydrogen sulfide and volatile organic compounds vapor, are major threats to the ecological environment safety and human health. Among the available technologies, gas sensing is a vital component, and has been widely studied in literature for early detection and warning. As a metal oxide semiconductor, zinc ferrite ($ZnFe_2O_4$) represents a kind of promising gas sensing material with a spinel structure, which also shows a fine gas sensing performance to reducing gases. Due to its great potentials and widespread applications, this article is intended to provide a review on the latest development in zinc ferrite based gas sensors. We first discuss the general gas sensing mechanism of $ZnFe_2O_4$ sensor. This is followed by a review of the recent progress about zinc ferrite based gas sensors from several aspects: different micro-morphology, element doping and heterostructure materials. In the end, we propose that combining $ZnFe_2O_4$ which provides unique microstructure (such as the multi-layer porous shells hollow structure), with the semiconductors such as graphene, which provide excellent physical properties. It is expected that the mentioned composite contributes to improving selectivity, long-term stability, and other sensing performance of sensors at room or low temperature.

Key Words: zinc ferrite, nanostructure, doping, heterojunction, reducing gas, gas sensing

1 Introduction

While the rapid development of modern industry has promoted unexperienced economic growth in human history, it brings about various toxic, harmful, flammable and explosive gases such as volatile organic compounds (VOCs) and hydrogen sulfide (H_2S), which pose a continuing threat to environmental safety and human health [1-2]. Therefore, gas analysis, detection and alarms are of great concern to the industry and the society at large. The conventional gas analysis methods such as high-performance liquid chromatography (HPLC) [3], spectrometry-gas chromatography (GC) [4-5] can detect gases accurately. Nonetheless, these methods have high requirements for advanced equipment, which makes these methods more appropriate for testing in a laboratory environment, and due to the complexity of the procedures, they are both time-consuming and expensive. As a result, the gas sensors that can be easily manufactured and conveniently deployed on site with low manufacturing and implementation costs have attracted great interests from both industry and government agencies. A stream of studies has shown that metal oxide semiconductor (MO) sensors are considered to be effective solutions to detection of harmful gases, owing to their advantages of high sensitivity, fast response and easy integration.

The MO gas sensing materials can be divided into two categories based on a number of types of metal oxides involved in the material: single and composite metal oxides. Single metal oxides have been widely studied as gas sensing materials. These include zinc oxide (ZnO) [6], tin oxide (SnO_2) [7], tungsten oxide (WO_3) [8-9], titanium oxide (TiO_2) [10] and iron oxide (Fe_2O_3) [11]. The high-performance gas sensors based on single metal oxides possess the characteristics of easy integration and good repeatability, and can effectively detect a variety of gases (CO, NH_3, O_3, etc.). However, the selectivity and recovery property of single-phase gas sensing materials for reducing

gases such as VOCs still need to be enhanced. In this regard, attempts were made to modify single metal oxides morphology to provide reactive activation energy or to form p-n heterojunctions through the doping of noble metal catalysts or the combination with other materials, resulting in enhanced sensing properties. For instance, the compound of two single metal oxides generated homogeneous or heterogeneous junctions, such as SnO_2/ZnO [12], ZnO/α-Fe_2O_3 [13] and WS_2/WO_3 [14]. In addition, the complex oxides such as spinel (AB_2O_4) [15-16] or perovskite (ABO_3) [17] show better sensing performance to certain gases than single oxides.

As a typical spinel ferrite, $ZnFe_2O_4$ is a semiconductor with a narrow band gap (~1.9 eV), which possesses various excellent properties. It has attracted much attention in the applications of gas sensors [18-19], catalyst [20], magnetic materials [21] and lithium battery materials [22]. In recent years, the preparation methods of $ZnFe_2O_4$ based gas sensing materials mainly include co-precipitation [23-24], sol-gel [25] and template synthesis method [26], which can prepare $ZnFe_2O_4$ nanomaterials with different morphology, such as nanorods, nanotubes, nano-thin films and core-shell microspheres. $ZnFe_2O_4$ based gas sensing materials mainly include pure $ZnFe_2O_4$ nanomaterials, metal element doping $ZnFe_2O_4$ and oxide - $ZnFe_2O_4$ composite materials, which are mostly used to detect reducing gases. Zinc ferrite based gas sensors reviewed in this paper belong to the semiconductor gas sensor family, which shows a response to reducing gas via converting chemical signals to electrical signals. In order to make a clear comparison, it is necessary to explain two vital properties of sensors, the one is response (S), all the definitions of which are listed in corresponding tables below, the other is response/recovery time ($\tau_{res.}/\tau_{rec.}$), which are generally defined as the time taken by the sensor to achieve 90% of the total resistance variation in the case of adsorption and desorption, respectively.

The rest of this review article is as follows: section 2 introduces the gas sensing mechanism of

$ZnFe_2O_4$; section 3, 4 and 5 provides a review of latest research progress in $ZnFe_2O_4$ based gas sensing materials for detecting reducing gases according to the types of gas sensing enhancement mechanism; section 6 makes a summary and prospect about this review.

2 Gas sensing mechanism

As a novel sensing material, zinc ferrite has excellent properties owing to its spinel crystal structure. The crystal structure of zinc ferrite is shown in Fig. 1 [27]. The O^{2-} in its crystal accumulate in face-centered cube, and the metal ions Zn^{2+} and Fe^{3+} are embedded in the tetrahedral and octahedral gaps composed of O^{2-}. It is easy to form defects inside or on the surface, such as oxygen vacancies, which is very favorable for gas sensitive materials. Moreover, the unique crystal structure of transition metal cations Zn^{2+} inserting into the $Fe^{2+}Fe^{3+}O_4$ structure performs well in the detection of reducing gas [28].

The response of $ZnFe_2O_4$ to the target gases depends on the complex interaction of the gas-solid interface, but there is no unified definition of the mechanism of gas sensors. A popular sensing mechanism of $ZnFe_2O_4$ sensors can be described as following: When $ZnFe_2O_4$ based sensor is exposed to air, oxygen molecules will adsorb on its surface and capture free electrons from its conduction band to form oxygen anions. The forms of oxygen anions depend on the operating temperature. When the operating temperature is below 147℃, the oxygen anions are mainly O_2^- (Eq. 2). O_2^- will be transformed into O^- (Eq. 3) with the increase of temperature. When the temperature is over 397℃, the oxygen anions are converted into O^{2-} (Eq. 4). The electron depletion layer (n-type) generates on the semiconductor surface due to the loss of electrons, which also gives rise to increased resistance of the sensor. When it is placed in a reduced gas atmosphere, the reaction, Eq. 6, will take place, which will decrease the electron depletion region, as well as the resistance of sensors.

For example, when $ZnFe_2O_4$ gas sensors detect acetone at the temperature of 147-397°C, there will be a reaction (Eq. 7), and Fig. 2 illustrates the corresponding mechanism. Moreover, if the working temperature or target gas is different, the reaction Eq. 6 may be different. The equations are as follows [1,37,52]:

$$O_2\ (gas) \leftrightarrow O_2\ (ads) \quad (1)$$

$$O_2\ (ads) + e^- \leftrightarrow O_2^-\ (ads) \quad T < 147°C \quad (2)$$

$$O_2^-\ (ads) + e^- \leftrightarrow O^-\ (ads) \quad 147°C < T < 397°C \quad (3)$$

$$O^-\ (ads) + e^- \leftrightarrow O^{2-}\ (ads) \quad T > 397°C \quad (4)$$

$$G\ (gas) \leftrightarrow G\ (ads) \quad (5)$$

$$G\ (ads) + O^- \rightarrow GO + e^- \quad 147°C < T < 397°C \quad (6)$$

$$C_3H_6O + 8O^- \rightarrow 3CO_2 + 3H_2O + 8e^- \quad (7)$$

The advantages of unique crystal structure and high surface activity of zinc ferrite make it a superior gas sensing material, especially for reducing gases or vapors. In addition, its surface oxygen adsorption activation energy is low (the activation energy represents the difficulty of reaction between adsorbed oxygen and target gas), which makes it easy to react with the reducing gases, showing a very high response. Due to the urgent demand for high-performance gas sensors, in addition to pure $ZnFe_2O_4$ nanomaterials, metal doped $ZnFe_2O_4$ mixed materials and hetero-structure gas sensing materials have been successively prepared [29-30]. The corresponding enhanced mechanism are briefly introduced as follows: the unique microstructure and high specific surface area of pure $ZnFe_2O_4$ nanomaterials provide enough sites for gas adsorption, which can improve the sensing performance effectively; the doping of noble metals (such as Ag, Pd, etc.) can further lower the potential barrier height of grain boundary and increase the diffusion or transfer rate of carrier; the heterostructure can regulate electron depletion region and potential barrier at its interface through the interaction of Fermi energy level and energy band to improve the gas sensing performance. The

specific gas sensing mechanisms for these new materials will be described in section 3 (materials with different nanostructures), section 4 (doped materials) and section 5 (hetero-structure materials).

3 Nanostructure

Nanomaterials with optimized size/dimension and suitable morphology show great potentials in gas sensing applications. The gas sensing performance of zinc ferrite can be affected by operating temperature [31], humidity [32] and gas concentration. In addition to external factors, the properties associated with $ZnFe_2O_4$ morphologies are also influencing factors, such as the specific surface area, contact area, porosity, grain size and the order of grain stacking and aggregation. In other words, different nano/microstructures, such as nanoparticles [33], nanorods [34] and micro/nanospheres [35], will affect the gas sensing characteristics of $ZnFe_2O_4$. Therefore, creating special forms and structures in $ZnFe_2O_4$ has been considered by researchers as a potential method to obtain the desired properties. Besides, porous $ZnFe_2O_4$ with the high specific surface area can provide more active vacancies, thus improving its surface effect and electron transfer efficiency, resulting in enhanced gas sensing properties. $ZnFe_2O_4$ materials with different morphologies can be synthesized by various preparation techniques. The following sections will review the latest work on different nanostructures and the special properties reported in the literature for $ZnFe_2O_4$ based sensor according to their nano/microstructures.

3.1 Nanoparticles

As the above mentioned, the proper grain size and specific surface area of $ZnFe_2O_4$ can improve sensing performance of sensors. Zhang et al. [36] synthesized $ZnFe_2O_4$ nanoparticles with good dispersion using the hydrothermal method. The reaction conditions played a significant role in the

phase and morphology of the prepared products, such as reaction time, temperature and molar ratio of raw materials. After reacting at 180°C for 12 h, the obtained $ZnFe_2O_4$ grains diameter is about 10 nm, along with a specific surface area of 115.6 $m^2 g^{-1}$. Compared with zinc oxide, zinc ferrite sensors showed better performance of acetone detection even working at a lower temperature (200°C). As shown in Fig. 3, compared with ZnO based sensor, the synthesized $ZnFe_2O_4$ nanoparticle also exhibited shorter response and recovery time. Darshane et al. [37] synthesized zinc ferrite nanoparticles via an environmentally friendly molten salt route. The synthesized nanoparticles were then coated on an alumina substrate with gold electrodes to test its response to H_2S. What is important, adding ionic salt substances as the precursor can inhibit the natural aggregation of grains due to thin walls formed around the nanoparticles, preventing sintering even at higher temperatures. When prepared at 700°C, the grain size of $ZnFe_2O_4$ was only from 15 nm to 20 nm, which suggests that the growth of particles at high temperatures can be controlled by binding the salt substances. When the working temperature was set at 250°C, $ZnFe_2O_4$ nanoparticles gas sensor showed fine response and selectivity to 200 ppm H_2S due to the proper grain size. This reported operating temperature was lower than other $ZnFe_2O_4$ synthesized without ionic salt.

To further reduce the operating temperature, nanoparticles can be combined with organic polymers [38-39]. Abu-Hani et al. [40] synthesized $ZnFe_2O_4$ nanoparticles using the co-precipitation method. The grains were uniformly distributed with the size of 3.6-6.4 nm. The synthesized zinc ferrite nanoparticles were then mixed into polymer solutions of polyvinyl alcohol (PVA) and glycerol ionic liquid (IL), which were cast into gas-sensitive layers by solution casting. At the temperature of 80°C, the PVA-IL-$ZnFe_2O_4$ gas sensing layer showed a good response to 300 ppm H_2S. Meanwhile, it possessed excellent selectivity, flexibility and good repeatability. It can be explained that polymer

solutions improved their electrical conductivity since glycerol ionic liquid possess good ionic conductivity. However, the sensor should be improved further to have a lower detection limit, in order to realize broad applications.

3.2 Nanorods/nanotubes

Compared with $ZnFe_2O_4$ nanoparticles, the materials with one-dimensional (1D) nanostructures, for instance, nanorods, nanotubes and nanowires, possess more active sites and gas diffusion structure, which can effectively transmit carriers. Zhu et al. [41] synthesized porous $ZnFe_2O_4$ nanorods using cetyltrimethylammonium bromide/water/cyclohexane/n-pentanol as the microemulsion system. The $ZnFe_2O_4$ nanorods synthesized were about 50 nm in diameter, which was composed of $ZnFe_2O_4$ nanocrystals (diameter: 5-10 nm) in a linear arrangement. Porous $ZnFe_2O_4$ nanorods showed better gas sensing properties than $ZnFe_2O_4$ nanoparticles at room temperature as ethanol sensors. This enhanced sensing performance is mainly owing to the porous nanorods distributing in random orientation and the existence of porous interconnection channels, which greatly increased the specific surface area of the nanorods, allowing an easier diffusion of target gas to be detected efficiently. At the same time, smaller $ZnFe_2O_4$ grains possess more active sites and their size might be similar to the thickness of electrons depleted region, which led to a certain enhancement of the response.

Cao et al. [42] prepared $ZnFe_2O_4$ nanorods via a solid-state chemical reaction. The specific surface area of the nanorods was 67.14 $m^2\ g^{-1}$. When detecting ethanol, the sensor demonstrated a fine response, selectivity, and long-term stability. The response value to 100 ppm ethanol was 29.1, and response/recovery time was only 2/7 s at 260ºC. Li et al. [43] reported $ZnFe_2O_4$ nanorods with a reticular pore structure, synthesized through an environmentally friendly and green hydrothermal method using $ZnFe_2(C_2O_4)_3$ as the template. It can be shown in Fig. 4, nanorods were composed of

small-sized nanoparticles, and there are a large number of pores on the surface. Moreover, the reticular pore structure provided the high specific surface area (82.01 m^2 g^{-1}). Porous $ZnFe_2O_4$ nanorods sensor showed fast response to acetone (at 260°C, the response and response/recovery time to 100 ppm acetone were 52.8 and 1/11 s, respectively). As shown in Fig. 4(f-g), the response showed good linearity as acetone concentration varied from 1 to 100 ppm. This excellent response is attributed to fine nanoparticle size, suitable pore size and reticular pore structure. However, when acetone concentration was above 100 ppm, the desorption capacity of the sensing materials was lower than its adsorption capacity, and the response tended to be stable.

In addition, $ZnFe_2O_4$ nanotubes and nanowires [44] as one-dimensional nanomaterials, are more used as electrode materials in the past, owing to their high specific capacity and improved cyclic stability. Due to the channel structure of the nanotubes, coupled with the relatively high specific surface area and good electron characteristics, they become a potential gas sensing material. In this regard, Zhang et al. [45] prepared $ZnFe_2O_4$ nanotubes by pyrolyzing PVA-assisted Zn/Fe nitrate gel using porous alumina as a template. The experimental results indicated that the concentration of PVA sol-gel precursor would affect the microstructure of $ZnFe_2O_4$ nanotubes, and the optimal concentration was determined as 0.25 mol/L. As we can see from Fig. 5, when the concentration became low, the broken and incomplete nanotubes would occur; when the concentration was too high, the diameter of nanotubes and its wall thickness would be unevenly distributed. With a concentration of PVA sol-gel precursor at 0.25 mol/L, the corresponding sensors showed fast response to volatile organics, such as acetone and ethanol, mainly owing to the small crystal size of nanotubes and their unique nanostructure. However, the selectivity, the operating temperature and the fabrication technique of this sensor still need to be improved, to find wider use in practical

applications.

3.3 Nanosheets

$ZnFe_2O_4$ nanosheets are two-dimensional nanomaterials. The nanosheets can provide more reaction sites and diffusion paths for the gases to be measured, thus enhancing its gas sensing properties. Gao et al. [46] synthesized $ZnFe_2O_4$ preliminary product using hydrothermal method with flake graphene as hard template. Porous $ZnFe_2O_4$ nanosheets were prepared after heat treatment at 450ºC for 2 h. $ZnFe_2O_4$ nanoparticles were also obtained using the hydrothermal method to make a comparison with porous $ZnFe_2O_4$ nanosheets. The nanosheets have a specific surface area of 99.3 m^2 g^{-1} (nanoparticles, 24.7 m^2 g^{-1}). The performance of $ZnFe_2O_4$ nanosheets and nanoparticles sensor proved that the former has a lower operating temperature (85ºC), a shorter response/recovery time as well as excellent selectivity. At 85ºC, the response value of $ZnFe_2O_4$ nanosheets sensor to 0.5 and 1 ppm H_2S were 11 and 39.8, respectively. Besides, the repeatability and stability of this sensor were good. The enhanced performance could be ascribed to high specific surface area and porous features of the $ZnFe_2O_4$ nanosheets, which exposed more vacancies to facilitate the diffusion of the target gas molecules, in addition, the two-dimensional structure effectively prevented the aggregation of nanoparticles.

Li et al. [47] grew ultra-thin $ZnFe_2O_4$ nanosheets (about 10 nm thick) on the outer surface of the hollow structure of ZnO through a room temperature solution reaction, which showed a double shell structure that can provide a high specific surface area, 53.8 m^2 g^{-1}, while hollow ZnO was only 13.7 m^2 g^{-1}. Simultaneously, the heterojunction generated by the composite material increased the initial resistance. We can conclude that among pure ZnO, $ZnFe_2O_4$ and ZnO/$ZnFe_2O_4$, detecting the various concentration of acetone at 250ºC, ZnO/$ZnFe_2O_4$ sensors showed better gas sensing performance.

The gas sensing mechanism and dynamic response of the three sensors to acetone are shown in Fig. 6.

3.4 Nanospheres

Generally, $ZnFe_2O_4$ nanospheres mainly include solid spheres and hollow spheres evolved from the core-shell structure, which possess characteristics of low density, high specific surface area, high surface activity and good stability [48-49]. It was suggested in the literature that to obtain a larger specific surface area, it is necessary to improve the size of nanoparticles (whose diameter is 10-20 nm) [50]. Nanospheres assembled by nanoparticles will obtain better size, larger specific surface area and higher sensitivity. Zhou et al. [51] adopted ethanol-ethylene glycol as a binary solvent and synthesized the precursor material by the solvent-thermal method without a template. Annealing at 400°C for 2 h, porous $ZnFe_2O_4$ nanospheres can be obtained. Then the paste sample was coated on the alumina tube to fabricate the sensitive layer and embedded in the tube with a nickel-chromium alloy coil for temperature control. Porous $ZnFe_2O_4$ nanospheres were assembled from a large number of nanoparticles. The pore size was mainly 10-20 nm and its specific surface area was 59.0 m^2 g^{-1}. The unique porous and spherical structure effectively enhance the acetone sensing performance of the sensor. Detecting 800 ppb acetone at 200°C, the response of $ZnFe_2O_4$ nanospheres could reach 1.5. Moreover, the response value to 11.8-30 ppm acetone was 2-2.5 times higher than $ZnFe_2O_4$ nanoparticles. Meanwhile, it was fast in response (9 s) but slow in recovery (272 s) for 30 ppm acetone. Dong et al. [52] synthesized monodispersed $ZnFe_2O_4$ nanospheres with a larger surface area (87.40 m^2 g^{-1}) using solvothermal synthesis method and studied its response to toluene gas at low concentration. When detecting 1 and 100 ppm toluene at 300°C, $ZnFe_2O_4$ nanospheres showed a response of 1.41 and 9.98 respectively. It also showed good linear sensing performance. Due to the

simple preparation method and excellent response, $ZnFe_2O_4$ nanospheres are considered as effective materials for detecting low concentration toluene gas.

The hierarchical structure or hollow sphere nanomaterials combined with low-dimensional subunits can provide more adsorption vacancy and effectively improve gas sensing properties. Zhou et al. [53] synthesized the Zn-Fe precursor by solvothermal method, which was then annealed (400ºC, 2h) to obtain nanosheet-assembled $ZnFe_2O_4$ hollow microspheres. The sensor was fabricated by coating the hollow microspheres material on alumina tube. The average thickness of the interconnected $ZnFe_2O_4$ nanosheets was 20 nm, and the diameter of the hollow microsphere was 0.9-1.1 μm. The hollow flower structure provided a large number of adsorption/reaction sites. Meanwhile, there existed many diffusion channels (pore size is mainly distributed from 2 nm to 50 nm). At 215ºC, the response value to 100 ppm acetone was 37.3, and it also demonstrated fine long-term stability. However, in the same conditions, the response of the ethanol was high (27.0). In other words, the selectivity needs to be further improved. The reaction mechanism of the gas sensing layer was explained by the semiconductor energy level model, as shown in Fig. 7. And its acetone sensing mechanism is as described in Section 2.

Qu et al. [54] synthesized $ZnFe_2O_4$ double shell microspheres using an aqueous solution system instead of an organic solvent system. It was proposed in this work that the heat treatment parameters would affect the sample structure, as shown in Table 1. Compared with the other two structures, $ZnFe_2O_4$ double shell hollow sphere showed better crystallinity and larger specific surface area, which can not only lower the operating temperature of the sensor, but also enhance gas sensing properties to acetone. As for the sensor, the response to 5 ppm acetone was 2.6 at 206ºC, the response/recovery time was 6 s and 10 s. In addition to this, the acetone limit of detection was 0.13

ppm, which was far below the danger value for life and health (20,000 ppm) and the diabetes diagnostic threshold (0.8 ppm).

In conclusion, different microstructures result in the change of many structural parameters of $ZnFe_2O_4$, such as specific surface area, pore size distribution and crystallinity, which further affects the sensing performance of the $ZnFe_2O_4$ gas sensor. With acetone as the target gas, $ZnFe_2O_4$ of different microstructure and their partial corresponding gas sensing properties are shown in Table 2.

4 Doping

To further optimize the structure and performance of $ZnFe_2O_4$, element doping, as an effective method, was investigated in a stream of works in literature. To this point, the research on the doping of spinel $ZnFe_2O_4$ mainly focused on the fields of electrode and magnetism [57-61], which shows improved performance. Until recent years, the new progress has been made in research on the effects of doping, especially the doping of metallic elements, on $ZnFe_2O_4$ gas sensing properties[62]. Not all metallic elements can be used for doping, the metallic elements with the donor (high valence) or acceptor (low valence) characteristics are more suitable for doping modification. There are mainly two existing forms of metallic elements. The first is utilizing the tetrahedral and octahedral interstices of $ZnFe_2O_4$ crystals, which allow the doping elements to enter the interstice to generate solid solution structure. The other is that doping elements replace Zn and Fe ions using displacement. It can be sure that doping can change the composition and microstructure of $ZnFe_2O_4$ (such as crystallinity, etc.), which will affect the reference resistance and sensing performance of $ZnFe_2O_4$ based gas sensors. In this section, we intend to review the research progress in element doped $ZnFe_2O_4$ and its influence on gas sensing properties.

4.1 metal element doping

The introduction of metallic elements, for example, vanadium (V), gold (Au), silver (Ag) and palladium (Pd), can generate an activation center on the surface of the semiconductor, and its unoccupied d orbit is able to accept electrons, which contributes to promoting charge separation and improving adsorption capacity, and finally improving the gas sensing performance [63]. Jiang et al. [30] synthesized $ZnFe_2O_4$ powder using a citrate pyrolysis method. Subsequently, the group obtained $ZnFe_2O_4$ doped with V derived from V_2O_5 dissolved in ammonia solution. They prepared a slurry and evenly coated it on Al_2O_3 tubes with Au electrodes and Pt to fabricate the gas sensing layer. The characterization results proved that the high-valency V^{5+} formed a solid solution in the interstice or substitution sites of the $ZnFe_2O_4$ crystal lattice, which enhanced its electronic and gas sensing properties. Only when detecting benzene gas or its derivative steam, the response increased significantly at high operating temperature, which may result from the catalytic oxidation effect of vanadium oxides for benzene and its derivatives. Therefore, V-doped $ZnFe_2O_4$ is not ideal in detecting ethanol and acetone, but it is attractive as the benzene and its derivatives gas sensor. However, future work to reduce the operating temperature is still needed for the practical application of this new technology. Zhang et al.[64] introduced Ag into nanosheets stacked $ZnFe_2O_4$ hollow structure via the hydrothermal method. With the increase of the contents of Ag, there was no obvious change in the sphere size while the surface structure was modified, as shown in Fig. 8(a-b). The spheres were composed of more and more nanoparticles rather than stacked sheets, which caused a decrease in specific surface area. At 175°C, 0.25 wt% Ag-$ZnFe_2O_4$ sensors showed better sensing performance than pure $ZnFe_2O_4$ sensors, as shown in Fig. 8 (c-f). The enhanced performance of 0.25 wt% Ag-$ZnFe_2O_4$ sensors was attributed to the proper hollow structure and activating effect of Ag. The Ag-$ZnFe_2O_4$ sensors should be a potential choice for the detection of low-ppm-level acetone.

However, although its gas selectivity was good and the effect of humidity was slight, the long-term stability needs to research and improve further.

While $ZnFe_2O_4$ works as a good sensing material towards H_2S [65], it also suffers from the same problem as V-$ZnFe_2O_4$ with high operating temperature. To lower the operating temperature, $ZnFe_2O_4$ gas sensing materials are modified with appropriate catalysts such as noble metals [66]. Yan et al. [67] obtained Au doped $ZnFe_2O_4$ microspheres using the chloroauric acid solution as the gold source, which was then treated by solvothermal method, annealing treatment and chemical etching process. The doping of Au did not change the spinel structure of $ZnFe_2O_4$, but the microsphere size changed irregularly with the increase of Au doping. When the Au-doping concentration were 0.5, 1, 1.5, 2 and 5 wt %, the microsphere size of Au-$ZnFe_2O_4$ were 2.15, 2.27, 2.32, 3.71 and 3.22 μm, respectively. It was confirmed that 2 wt% Au-$ZnFe_2O_4$ microsphere possessed a yolk-shell structure with the shell thickness of about 630 nm, coupled with a porous and rough surface structure. This unique surface improved gas transmission efficiency and gas adsorption effectiveness, thus improving the gas sensitivity of the sensor. In addition, at room temperature, the Au of different concentration doped $ZnFe_2O_4$ sensor showed good selectivity and stability to H_2S. As Au doping concentration increased, the response of the Au-$ZnFe_2O_4$ sensor to H_2S was enhanced, as shown in Table 3, 2 wt% Au-$ZnFe_2O_4$ showed the best gas sensing performance. In addition, the response/recovery time was 46 s and 629 s. In view of the fine properties of the gas sensor based on $ZnFe_2O_4$ nanosheets, combining element doping method with improved microstructure is a feasible method to enhance the sensor performance.

4.2 Mixed metal ferrite

Compounds of the type MFe_2O_4 realize the applications in the sensors field due to their good

surface activity (M = Mg, Cu, Zn, Ni, Co, etc.). Ebrahimi et al. [69] introduced nickel (Ni) to $ZnFe_2O_4$ by co-precipitation method, subsequently, they obtained the $Ni_{0.5}Zn_{0.5}Fe_2O_4$ nanoparticles with a diameter less than 20 nm after annealing treatment (500ºC, 3 h). The synthesized structure remained as the typical face-centered cubic spinel structure. The $Ni_{0.5}Zn_{0.5}Fe_2O_4$ powder was pressed into the cylinder equipped with the copper electrode to fabricate a gas sensor. At 350ºC, it was capable of detecting 80-200 ppm acetonitrile, with a corresponding response of 2.1 for the 200 ppm acetonitrile. However, since the sensor response is defined via the voltage variable, the sensor capacity reached the saturation state when the gas concentration reaches 200 ppm, resulting in the limited detection range.

To improve the sensing performance or lower the operating temperature, it is helpful to obtain unique microstructure, adjust the portion of the mixed metallic element. Mukherjee et al. [70-71] improved the electronic characteristics of ferrites by adjusting their surface to volume ratios. They synthesized one-dimensional (1D) $Mg_{0.5}Zn_{0.5}Fe_2O_4$ hollow nanotubes using wet chemistry with porous anodized aluminum as the template. The nanotubes have a length of 5-10 μm, a pore diameter of about 180 nm, and the thickness of wall was 15-20 nm. The nanotubes were subsequently dispersed in ethanol, and the obtained suspension was directly coated on the fused quartz substrate to fabricate the nanotube sensor, which can detect H_2 and CO. Owing to large amounts of adsorbed oxygen on the nanotube surface, however, it behaved p-type conducting semiconductor, and the holes became the main charge carrier. At 350ºC, the response to 10 ppm and 1660 ppm H_2 were 10% and 66%, respectively, and the response to 1660 ppm CO was 25%. Due to the fine hydrogen sensing performance of the sensor, the group further studied the H_2 sensing properties of $Mg_{0.5}Zn_{0.5}Fe_2O_4$ thin films, and it was found that the thickness of the film affects the performance of the sensor. The

thickness of the film was defined by the number of coating times, and when it was 15 or 30, the sensor response to 1660 ppm H_2 reached 76% at 250ºC. What is important, it also obtained reproducible sensing characteristics. The fine sensing performance may benefit from the nano-crystalline nature of these films. Mondal et al. [72] synthesized $Cu_{0.5}Ni_{0.25}Zn_{0.25}Fe_2O_4$ (CNZ1) and $Cu_{0.25}Ni_{0.5}Zn_{0.25}Fe_2O_4$ (CNZ2) via co-precipitation method, the two sensors showed fine response to acetone and ethanol at room temperature. It was concluded that the introduction of copper improved the sensitivity of acetone to 77%, while the introduction of nickel improved the sensitivity of ethanol to 75%.

Table 4 shows the comparison of all above-discussed gas sensing materials. Although the sensitivity of the sensor has been improved to some extent, the concentration range of the gas detected by such mixed metal ferrite is limited, and the response/recovery time is relatively long. It is proposed that combining with other metal oxides or two-dimensional nanomaterials shall be attempted to further enhance these properties.

5 Heterostructure

As concluded in section 3 and 4, the gas sensing properties of $ZnFe_2O_4$ sensor can be enhanced to certain degrees via adjusting its morphology or doping elements. To further obtain the desired performance, researchers developed various $ZnFe_2O_4$ composites, which is more applied in photocatalysis and sensing fields [73-75]. In this regard, current research and applications mainly focus on combining the transition metal oxide (ZnO, Fe_2O_3) with $ZnFe_2O_4$ to synthesize desired composites. Specifically, ZnO itself is also a good gas sensing material detecting reducing gas [76-77], as a result of this, ZnO/$ZnFe_2O_4$ heterostructure nanomaterials are more heavily studied by researchers in literature. The latest development in this field was combining carbon materials such as

graphene with $ZnFe_2O_4$ composites. As such, the goal of this section is to review the latest works on $ZnFe_2O_4$ composites and to introduce the effects of the above two types of composites on gas sensing properties.

5.1 ZnO/$ZnFe_2O_4$

When ZnO and $ZnFe_2O_4$ are combined, the electron depletion layer will be generated at contact interface because of the difference in both energy band gaps and work functions of two components. Fig. 9 shows an energy band structure of the composite, which explains the gas sensing mechanism (take acetone for example). The heterostructure effectively enhances the electronic properties and gas-sensitive properties of the material [79,84]. Wang et al. [78] synthesized $ZnFe_2O_4$/ZnO nanomaterial using the low-temperature hydrothermal method. The slurry of the synthesized composite was then coated on an alumina tube with gold electrodes and platinum wire. The obtained $ZnFe_2O_4$/ZnO composite showed a rod structure with a length of 140-410 nm and diameter of 9.4-34.7 nm. The loose and porous microstructure of this one dimensional and heterogeneous composite contributed to enhancing sensing performance. At the relative humidity of about 14% and the temperature of 260ºC, the $ZnFe_2O_4$/ZnO sensor for n-butyl alcohol showed fine performance: high sensitivity and short response/recovery time.

More works found in the literature attempted to create and study special microstructures in the composite materials, which can greatly enhance gas sensing performance. Ma et al. [79] dissolved ZnO nanorods in $FeSO_4$ aqueous solution. Subsequently, ZnO/$ZnFe_2O_4$ nanoforest were obtained after calcining at 500ºC in air. This composite material is characterized as $ZnFe_2O_4$ nanosheets that were covered on the surface of ZnO nanorods. It was then made into a paste and coated on the Al_2O_3 substrate to prepare the sensing layer. The microstructure of the final product could be influenced by

the dosage of $FeSO_4$ aqueous solution and dissolution time, and the ideal product could be prepared when the dosage and dissolution time was 0.2 mol and 30 minutes, respectively. The sensor showed a fine response to ethanol at 275ºC, which was attributed to the unique morphology and the heterostructure it carries. Liu et al. [80] washed ZnO products three times with ferric nitrate solution, and ZnO/$ZnFe_2O_4$ were then obtained after annealing at 500ºC for 2h in air. The morphology of the synthesized composite showed $ZnFe_2O_4$ nanoparticles attached to flower ZnO. Owing to the low-agglomerated flower $ZnFe_2O_4$/ZnO microstructure, synergistic effect and the heterojunction formed at the interface between the $ZnFe_2O_4$ and ZnO, $ZnFe_2O_4$/ZnO sensor exhibited better acetone sensing performance. It showed a higher response and fast response/recovery. Moreover, the sensor could detect 1 ppm acetone with the response of 1.3.

Although the research on ZnO/$ZnFe_2O_4$ composite produced promising results, it should be noted that the performance and application range of ZnO/$ZnFe_2O_4$ composite is limited, due to the weak interface, low density, small specific surface area, and the high energy consumption. To remedy these shortcomings, hollow nanostructures with internal voids and functional shells were further investigated by researchers, and applying their special properties in applications such as catalysis and energy storage/conversion [81-83]. These special hollow structures could increase the specific surface area thus improving the permeability of the ZnO/$ZnFe_2O_4$ composite material and producing improved sensing properties. Zhang and co-workers [84] synthesized ZnO/$ZnFe_2O_4$ hollow spheres by a simple hydrothermal method using carbon balls as templates, in which porous spherical shells (thickness about 30 nm) were formed after carbon ball templates were calcined and removed in air. Furthermore, ZnO/$ZnFe_2O_4$ nanoparticles were synthesized to compare with the performance of the hollow sphere gas sensor. The comparison showed that the hollow sphere sensor obtained a higher

response to acetone and a shorter response/recovery time (5.5, 7.1 s / 10.8 s). These enhanced properties were attributed to the porous hollow structure which improved electrical properties, and the properties of p-n heterojunction. Wang et al. [85] prepared $ZnO/ZnFe_2O_4$ nanocage via Metal-Organic Frameworks (MOF). Firstly, Fe (III) MOF-5 nanocage precursor was synthesized using refluxing process; the product was then collected after annealing in air. The specific surface area of the nanocage was 48.4 m^2g^{-1}. Due to the heterojunction and its unique structure, as a gas sensor, it could detect 1 ppm acetone vapor. The response was also superior to pure $ZnFe_2O_4$ and $ZnO/ZnFe_2O_4$ sensors with other structures. However, the reported operating temperature was still high (290ºC). Song et al. [86] synthesized $Zn_3[Fe(CN)_6]_2 \cdot xH_2O$, a prussian blue analogue precursor, using coprecipitation, subsequently, annealing at 550ºC for 2 h to obtain $ZnO/ZnFe_2O_4$ three-layer shell hollow microspheres (ZZFO TSHMs), as shown in Fig. 10. The hollow microsphere showed a high specific surface area (62.4 $m^2\ g^{-1}$). Meanwhile, the hollow interior and the gap between the three-layer porous shells facilitated the diffusion of the target gas. The ZZFO TSHMs acetone sensor showed high sensitivity, fast response, good stability and selectivity at low temperature (140ºC).

5.2 Graphene/$ZnFe_2O_4$

Graphene as a new carbon material has both high specific surface area and unique structure where sp^2 hybridized carbon atoms are tightly wrapped in the two-dimensional honeycomb lattice. Coupled with its excellent thermal conductivity, electrical conductivity and high mechanical strength, graphene finds applications in thermal [87], electrical [88] and mechanical [89] fields. With no surprise, graphene is also a popular material investigated in gas sensing areas. Some works include the attempt by Hafiz et al. [90] where a room temperature carbon dioxide gas sensor was produced by reducing the graphene oxide with hydrogen plasma. Seekaew et al. [91] deposited graphene onto a nickel-based

digital electrode through chemical gas phase transfer to prepare a fine room-temperature NO_2 gas sensor based on double-layer graphene.

In recent years, graphene-based room temperature sensors have attracted extensive attention. Liu et al. [92] synthesized rGO/In_2O_3 gas sensing material via a hydrothermal method. It was reported that that 3 wt% rGO/In_2O_3 composite sensor showed an extremely low detection limit (10 ppb NO_2), excellent selectivity, stability and rapid response. Zhang et al. [93] synthesized 1.0 wt% rGO/α-Fe_2O_3 using the hydrothermal method, with a structure where α-Fe_2O_3 cubes adhered evenly to both sides of the rGO sheet. When tested with 100 ppm acetone vapor at 225°C (while α-Fe_2O_3 was tested at 237.5°C), the sensor showed the response of 13.9, which was about 2.5 times that of α-Fe_2O_3. Its response time was also decreased to 2 s. The works mentioned above support the hypothesis that the combination of metal oxide sensors with graphene or its derivatives can reduce the operating temperature and enhance sensing performance. This could be explained by two main advantages this combination brings to the sensor: 1) metal oxide nanoparticles prevent graphene from agglomeration, resulting in a larger specific surface area. 2) graphene or its derivatives improves the conductivity of the composite, provides more adsorption sites and contributes to the formation of local heterojunctions [94].

Aiming to improve the response of $ZnFe_2O_4$ based sensors and further reduce their limit of detection, graphene or its derivatives were investigated by a few latest work found in literature. Until now, the widely used and simple preparation method is solvothermal synthesis method [95-96]. The synthesis process of $ZnFe_2O_4$/rGO is shown in Fig. 11. During the procedure, Zn^{2+}/Fe^{3+}-GO were firstly obtained owing to the existence of the oxygen-containing functional groups, subsequently, it was in-situ converted to $ZnFe_2O_4$ on the graphene matrix, meanwhile, the GO was reduced to rGO.

Liu et al. [96] used hydrazine hydrate to reduce graphene oxide. Thereafter, rGO/$ZnFe_2O_4$ composites with different proportions were synthesized via a solvothermal method. The morphology of the synthesized composite was characterized as $ZnFe_2O_4$ nanoparticles adhered to rGO sheets. It was found that 0.125 wt% rGO/$ZnFe_2O_4$ sensor showed rapid response and good stability to acetone at 275ºC, these following reactions (Eqs. 8,9,7) may occur in the surface reaction. It should be noted that, although the response was improved, the selectivity and operating temperature of this composite still represents a problem for practical applications.

$$e^- (ZnFe_2O_4 \text{ or } G - ZnFe_2O_4) + O_2 \rightarrow O_2^- \quad (8)$$

$$e^- (ZnFe_2O_4 \text{ or } G - ZnFe_2O_4) + O_2^- \rightarrow 2O^- \quad (9)$$

$$C_3H_6O + 8O^- \rightarrow 3CO_2 + 3H_2O + 8e^- \quad (7)$$

However, the current composite materials of zinc ferrite and graphene are mostly applied in the catalyst and wave absorbing materials [97-98]. As for gas sensing, further study and development are needed. It is so proposed that the performance of the graphene/$ZnFe_2O_4$ composite sensor can be improved by changing the microstructure of zinc ferrite or the structural parameters of graphene, such as the number of layers and sensitization processing. The morphology and gas sensing performance of $ZnFe_2O_4$ composites reported in the literature is listed in Table 5.

6 Summary and prospect

Owing to the spinel structure and excellent sensing performance of $ZnFe_2O_4$, there have been many reports on $ZnFe_2O_4$ research in recent years. Various nanostructure materials based on $ZnFe_2O_4$ are widely developed and applied in the fields of photoelectricity, magnetism, energy storage, catalyst and sensors. Among them, zinc ferrite gas sensor is simple to prepare, inexpensive, and sensitive to a variety of inflammable and explosive, toxic and harmful reducing gases. In this article, the research progress in $ZnFe_2O_4$ based gas sensors was reviewed from three aspects: nanostructure,

element doping and heterostructure.

Since the gas sensing process of $ZnFe_2O_4$ sensor is highly dependent on surface conduction effect, the difference in microstructure will lead to changes in grain size, specific surface area and porosity of $ZnFe_2O_4$ nanomaterials, which further affect the gas sensing performance of such sensors. The metal element doping of $ZnFe_2O_4$ improves the specific surface area on the basis of preserving the original crystal structure and offers the activation energy. As for the composite, the heterojunction is formed at the interface between different materials, and the response of sensor is adjusted mainly through the function of the formed electron depletion layer. By comparison, it can be found that improving the microstructure, proper metal element doping or material compounding can improve sensing performance of $ZnFe_2O_4$ based gas sensors to a certain extent. There are still problems such as high power consumption (owing to high operating temperature) and long recovery time, which are unfavorable for certain practical applications, such as the detection of diabetes (low-ppm acetone). To realize stable room temperature or low-temperature detection and rapid recovery of such sensors, new research directions are needed. Some new research has been done, such as the work by Raut et al. [101], $ZnFe_2O_4$ were able to reduce the operating temperature treated by gamma-ray irradiation; Sutka et al. [102] concluded that controlling iron stoichiometry could help improving gas sensing performance of spinel ferrite complex semiconductor. We suggest that the above reviewed three aspects can be combined to attack the requirement of high response and low operating temperatures. This includes but is not limited to: 1) improving the microstructure of $ZnFe_2O_4$ or controlling iron stoichiometry, 2) the composite of multi-layer porous shell $ZnFe_2O_4$ or hollow sphere with two-dimensional nanomaterials, such as reduced graphene oxide, molybdenum disulfide, 3) the multi-component hybrids, such as noble metal nanoparticles-$ZnFe_2O_4$-reduced graphene oxide

hybrids.

Acknowledgments

This work is supported by the Intergovernmental International Science and Technology Innovation Cooperation on the National Key Research and Development Program of China under Grant No. 2017YFE0115900, the Natural Science Foundation of China under Grant No. 51402255 and 51872254 and Yangzhou Science Fund for Distinguished Young Scholars under Grant No. YZ2017096.

References

1. N.V. Hoang, C.M. Hung, N.D. Hoa, N.V. Duy, N.V. Hieu, Facile on-chip electrospinning of $ZnFe_2O_4$ nanofiber sensors with excellent sensing performance to H_2S down ppb level, J. Hazard. Mater. 360 (2018) 6-16. https://doi.org/10.1016/j.jhazmat.2018.07.084.
2. S. Rasouli Jamnani, H. Milani Moghaddam, S.G. Leonardi, G. Neri, Enhanced selective catalytic wet oxidation of H_2S to S over Ce-Fe/MgO catalysts at ambient temperature, Ceram. Int. 44 (2018) 16953-16959. https://doi.org/10.1016/j.ceramint.2018.06.136.
3. F. Villanueva, A. Tapia, A. Notario, J. Albaladejo, E. Martínez, Ambient levels and temporal trends of VOCs, including carbonyl compounds, and ozone at Cabañeros National Park border, Atmos. Environ. 85 (2014) 256-265. https://doi.org/10.1016/j.atmosenv.2013.12.015.
4. T. Saidi, O. Zaim, M. Moufid, N.E. Bari, R. Ionescu, B. Bouchikhi, Exhaled breath analysis using electronic nose and gas chromatography-mass spectrometry for non-invasive diagnosis of chronic kidney disease, diabetes mellitus and healthy subjects, Sens. Actuators, B 257 (2018) 178-188. https://doi.org/10.1016/j.snb.2017.10.178.
5. A.L. Moriaux, R. Vallon, B. Parvitte, V. Zeninari, G. Liger-Belair, C. Cilindre, Monitoring gas-phase CO_2 in the headspace of champagne glasses through combined diode laser spectrometry and micro-gas chromatography analysis, Food Chem. 264 (2018) 255-262. https://doi.org/10.1016/j.foodchem.2018.04.094.
6. X. Geng, C. Zhang, Y.F. Luo, M. Debliquy, Flexible NO_2 gas sensors based on sheet-like hierarchical ZnO_{1-x} coatings deposited on polypropylene papers by suspension flame spraying, J. Taiwan Inst. Chem. Eng. 75 (2017) 280-286. https://doi.org/10.1016/j.jtice.2017.03.021.
7. B.G. Kim, D.G. Lim, J.H. Park, Y.J. Choi, J.G. Park, In-situ bridging of SnO_2 nanowires between the electrodes and their NO_2 gas sensing characteristics, Appl. Surf. Sci. 257 (2011) 4715-4718. https://doi.org/10.1016/j.apsusc.2010.12.137.
8. C. Zhang, X. Geng, M. Olivier, H.L. Liao, M. Debliquy, Solution precursor plasma-sprayed tungsten oxide coatings for nitrogen dioxide detection, Ceram. Int. 40 (2014) 11427-11431. https://doi.org/10.1016/j.ceramint.2014.03.109.
9. E.M. Preiß, A. Krauß, V. Kekkonen, N. Barsan, H. Seidel, Characterization of WO_3 thin films prepared by picosecond laser deposition for gas sensing, Sens. Actuators, B 248 (2017) 153-159.

https://doi.org/10.1016/j.snb.2017.03.096.
10. J. Nisar, Z. Topalian, A.D. Sarkar, L. Österlund, R. Ahuja, TiO_2-based gas sensor: a possible application to SO_2, ACS Appl. Mater. Interfaces 5 (2013) 8516-8522. https://doi.org/10.1021/am4018835.
11. S. Liang, J.P. Li, F. Wang, J.L. Qin, X.Y. Lai, X.M. Jiang, Highly sensitive acetone gas sensor based on ultrafine - Fe_2O_3 nanoparticles, Sens. Actuators, B 238 (2017) 923-927. https://doi.org/10.1016/j.snb.2016.06.144.
12. D.Y. Fu, C.L. Zhu, X.T. Zhang, C.Y. Li, Y.J. Chen, Two-dimensional net-like SnO_2/ZnO heteronanostructures for high-performance H_2S gas sensor, J. Mater. Chem. A 4 (2016) 1390-1398. https://doi.org/10.1039/C5TA09190J.
13. X. Zhou, Y. Xiao, M. Wang, P. Sun, F.M. Liu, X.S. Liang, X.W. Li, G.Y. Lu, Highly enhanced sensing properties for ZnO nanoparticle-decorated round-edged α-Fe_2O_3 hexahedrons, ACS Appl. Mater. Interfaces 7 (2015) 8743-8749. https://doi.org/10.1021/acsami.5b01071.
14. F. Perrozzi, S.M. Emamjomeh, V. Paolucci, G. Taglieri, L. Ottaviano, C. Cantalini, Thermal stability of WS_2 flakes and gas sensing properties of WS_2/WO_3 composite to H_2, NH_3 and NO_2, Sens. Actuators, B 243 (2017) 812-822. https://doi.org/10.1016/j.snb.2016.12.069.
15. A. Sutka, K.A. Gross, Spinel ferrite oxide semiconductor gas sensors, Sens. Actuators, B 222 (2016) 95-105. https://doi.org/10.1016/j.snb.2015.08.027.
16. J.M. Kwon, J.H. Kim, S.H. Kang, C.J. Choi, J.A. Rajesh, K.S. Ahn, Facile hydrothermal synthesis of cubic spinel AB_2O_4 type $MnFe_2O_4$ nanocrystallites and their electrochemical performance, Appl. Surf. Sci. 413(2017) 83-91. https://doi.org/10.1016/j.apsusc.2017.04.022.
17. L. Gildo-Ortiz, H. Guillén-Bonilla, V.M. Rodríguez-Betancourtt, O. Blanco-Alonso, A. Guillén-Bonilla, J. Santoyo-Salazar, I.C. Romero-Ibarra, J. Reyes-Gómez, Key processing of porous and fibrous $LaCoO_3$ nanostructures for successful CO and propane sensing, Ceram. Int. 44 (2018) 15402-15410. https://doi.org/10.1016/j.ceramint.2018.05.192.
18. J.J. You, X. Chen, B.B. Zheng, X. Geng, C. Zhang, Suspension plasma-sprayed $ZnFe_2O_4$ nanostructured coatings for ppm-level acetone detection, J. Therm. Spray Tech. 26 (2017) 728-734. https://doi.org/10.1007/s11666-017-0536-7.
19. X.F. Chu, X.Q. Liu, G.Y. Meng, Preparation and gas sensitivity properties of $ZnFe_2O_4$ semiconductors, Sens. Actuators, B 55 (1999) 19-22. https://doi.org/10.1016/S0925-4005(99)00033-7.
20. G.Q Hou, Y.K. Li, W.J. An, S.J. Gao, W.L. Zhang, W.Q. Cui, Fabrication and photocatalytic activity of magnetic core@shell $ZnFe_2O_4$@ Ag_3PO_4 heterojunction. Mater. Sci. Semicond. Process. 63 (2017) 261-268. https://doi.org/10.1016/j.mssp.2017.02.033.
21. D.W. Guo, C.J. Jiang, X.L. Fan, D.S. Xue, Thermal annealing effect on structural and magnetic properties of $ZnFe_2O_4$ thin films deposited by magnetron sputtering, Appl. Surf. Sci. 307 (2014) 576-578. https://doi.org/10.1016/j.apsusc.2014.04.075.
22. X.B. Zhong, Z.Z Yang, H.Y. Wang, L. Lu, B. Jin, M. Zha, Q.C. Jiang, A novel approach to facilely synthesize mesoporous $ZnFe_2O_4$ nanorods for lithium ion batteries, J. Power. Sources 306 (2016) 718-723. https://doi.org/10.1016/j.jpowsour.2015.12.102.
23. M.G. Naseri, E.B. Saiona, M. Hashima, A.H. Shaari, H.A. Ahangar, Synthesis and characterization of zinc ferrite nanoparticles by a thermal treatment method, Solid State Comm. 151 (2011) 1031-1035. https://doi.org/10.1016/j.ssc.2011.04.018.
24. J.Y. Patil, D.Y. Nadargi, J.L. Gurav, I.S. Mulla, S.S. Suryavanshi, Glycine combusted $ZnFe_2O_4$ gas sensor: Evaluation of structural, morphological and gas response properties, Ceram. Int. 40 (2014) 10607-10613. https://doi.org/10.1016/j.ceramint.2014.03.041.

25. A. Singh, AJ. Singh, S. Singh, P. Tandon, B.C. Yadav, R.R. Yadav, Synthesis, characterization and performance of zinc ferrite nanorods for room temperature sensing applications, J. Alloys Compd. 618 (2015) 475-483. https://doi.org/10.1016/j.jallcom.2014.08.190.
26. B.J. Liu, X.Y. Li, Q.D. Zhao, Y. Hou, G.H. Chen, Self-templated Formation of $ZnFe_2O_4$ Double-shelled hollow microspheres for photocatalytic degradation of gaseous o-dichlorobenzene, J. Mater. Chem.. A 5 (2017) 8909-8015. https://doi.org/10.1039/c7ta02048a.
27. Rachna, N.B. Singh, A. Agarwal, Preparation, characterization, properties and applications of nano zinc ferrite, Mater. Today : Proc. 5 (2018) 9148-9155. https://doi.org/10.1016/j.matpr.2017.10.035.
28. D. Mathew, R. Juang, An overview of the structure and magnetism of spinel ferrite nanoparticles and their synthesis in microemulsions, Chem. Eng. J. 129 (2007) 51-65. https://doi.org/10.1016/j.cej.2006.11.001.
29. W.H. Li, X.F. Wu, J.Y. Chen, Y. Gong, N. Han, Y.F. Chen, Abnormal n-p-n type conductivity transition of hollow ZnO/$ZnFe_2O_4$ nanostructures during gas sensing process: The role of ZnO-$ZnFe_2O_4$ hetero-interface, Sens. Actuators, B 253 (2017) 144-155. https://doi.org/10.1016/j.snb.2017.06.131.
30. Y. Jiang, W.L. Song, C.S. Xie, A.H. Wang, D.W. Zeng, M.L. Hu, Electrical conductivity and gas sensitivity to VOCs of V-doped $ZnFe_2O_4$ nanoparticles, Mater. Lett. 60 (2006) 1374-1378. https://doi.org/10.1016/j.matlet.2005.11.032.
31. H.R. Yang, X.J. Bai, P. Hao, J. Tian, Y.Y. Bo, X.Z. Wang, H. Liu, A simple gas sensor based on zinc ferrite hollow spheres: Highly sensitivity, excellent selectivity and long-term stability, Sens. Actuators, B 280 (2019) 34-40. https://doi.org/10.1016/j.snb.2018.10.056.
32. X.L. Xu, L.B. Xiao, N.O. Haugen, Z. Wu, Y.M. Jia, W.J. Zhong, J. Zou, High humidity response property of sol-gel synthesized $ZnFe_2O_4$ films, Mater. Lett. 213 (2018) 266-268. https://doi.org/10.1016/j.matlet.2017.11.092.
33. H.J. Zhang, F. Meng, L. Liu, Y. Chen, P. Wang, Highly sensitive H_2S sensor based on solvothermally prepared spinel $ZnFe_2O_4$ nanoparticles, J. Alloys Compd. 764 (2018) 147-154. https://doi.org/10.1016/j.jallcom.2018.06.052.
34. M.M. Rahman, S.B. Khan, M. Faisal, A.M. Asiri, K.A. Alamry, Highly sensitive formaldehyde chemical sensor based on hydrothermally prepared spinel $ZnFe_2O_4$ nanorods, Sens. Actuators, B 171-172 (2012) 932-937. https://doi.org/10.1016/j.snb.2012.06.006.
35. Z.M. Li, X.Y. Lai, H. Wang, D. Mao, C.J. Xing, D. Wang, General synthesis of homogeneous hollow core-shell ferrite microspheres, J. Phys. Chem. C 113 (2009) 2792-2797. https://doi.org/10.1021/jp8094787.
36. J. Zhang, J.M. Song, H.L. Niu, C.J. Mao, S.Y. Zhang, Y.H. Shen, $ZnFe_2O_4$ nanoparticles: Synthesis, characterization, and enhanced gas sensing property for acetone, Sens. Actuators, B 221 (2015) 55-62. https://doi.org/10.1016/j.snb.2015.06.040.
37. S.L. Darshane, R.G. Deshmukh, S.S. Suryavanshi, I.S. Mulla, Gas-sensing properties of zinc ferrite nanoparticles synthesized by the molten-salt route, J. Am. Ceram. Soc. 91 (2008) 2724-2726. https://doi.org/10.1111/j.1551-2916.2008.02475.x.
38. Daneshkhah, S. Shrestha, M. Agarwal, K. Varahramyan, Poly (vinylidene fluoride-hexafluoropropylene) composite sensors for volatile organic compounds detection in breath, Sens. Actuators, B 221 (2015) 635-643. https://doi.org/10.1016/j.snb.2015.06.145.
39. E.A. Khudaish, F. Al-Nofli, J.A. Rather, M. Al-Hinaai, K. Laxman, H.H. Kyaw, S. Al-Harthy, Sensitive and selective dopamine sensor based on novel conjugated polymer decorated with gold nanoparticles, J. Electroanal. Chem. 761 (2016) 80-88. https://doi.org/10.1016/j.jelechem.2015.12.011.
40. A.F.S. Abu-Hani, S.T. Mahmoud, F. Awwad, A.I. Ayesh, Design, fabrication, and characterization of portable gas sensors based on spinel ferrite nanoparticles embedded in organic membranes, Sens. Actuators, B 241

(2017) 1179-1187. https://doi.org/10.1016/j.snb.2016.10.016.
41. H.L. Zhu, X.Y. Gu, D.T. Zuo, Z.K. Wang, N.Y. Wang, K.H. Yao, Microemulsion-based synthesis of porous zinc ferrite nanorods and its application in a room-temperature ethanol sensor, Nanotechnol. 19 (2008) 405-503. https://doi.org/10.1088/0957-4484/19/40/405503.
42. Y.L. Cao, H.Y. Qin, X.J. Niu, D.Z. Jia, Simple solid-state chemical synthesis and gas-sensing properties of spinel ferrite materials with different morphologies, Ceram. Int. 42 (2016) 10697-10703. https://doi.org/10.1016/j.ceramint.2016.03.184.
43. L. Li, J.F. Tan, M.H. Dun, X.T. Huang, Porous $ZnFe_2O_4$ nanorods with net-worked nanostructure for highly sensor response and fast response acetone gas sensor, Sens. Actuators, B 248 (2017) 85-91. https://doi.org/10.1016/j.snb.2017.03.119
44. J.G. Kim, Y.G. Kim, Y.S. Noh, W.B. Kim, Formation of carbon-coated $ZnFe_2O_4$ nanowires and their highly reversible lithium storage properties, RSC Adv. 4 (2014) 27714-27721. https://doi.org/10.1039/c4ra02095b.
45. G.Y. Zhang, C.S. Li, F.Y. Cheng, J. Chen, $ZnFe_2O_4$ tubes: Synthesis and application to gas sensors with high sensitivity and low-energy consumption, Sens. Actuators, B 120 (2007) 403-410. https://doi.org/10.1016/j.snb.2006.02.034
46. X.M. Gao, Y. Sun, C.L. Zhu, C.Y. Li, Q.Y. Ouyang, Y.J. Chen, Highly sensitive and selective H_2S sensor based on porous $ZnFe_2O_4$ nanosheets, Sens. Actuators, B 246 (2007) 662-672. https://doi.org/10.1016/j.snb.2017.02.100.
47. X.W. Li, C. Wang, H. Guo, P. Sun, F.M. Liu, X.S. Liang, G.Y. Lu, Double-shell architectures of $ZnFe_2O_4$ Nanosheets on ZnO hollow spheres for high-performance gas sensors, ACS Appl. Mater. Interfaces 7 (2015) 17811-17818. https://doi.org/10.1021/acsami.5b04118.
48. X. Zhou, B.Q. Wang, H.B. Sun, C. Wang, P. Sun, X.W. Li, X.L. Hu, G.Y. Lu, Template-free synthesis of hierarchical $ZnFe_2O_4$ yolk-shell microspheres for high-sensitivity acetone sensors, Nanoscale 8 (2016) 5446-5453. https://doi.org/10.1039/c5nr06308f.
49. T. Liu, J.Y. Liu, Q. Liu, R.M. Li, H.Q. Zhang, X.Y. Jing, J. Wang, Shape-controlled fabrication and enhanced gas sensing properties of uniform sphere-like $ZnFe_2O_4$ hierarchical architectures, Sens. Actuators, B 250 (2017) 111-120. https://doi.org/10.1016/j.snb.2017.04.163.
50. P.Z. Gu, L.J. Cui, Y.Q. Wang, M. Lv, B.Y. Wang, X.S. Zhao, Facile synthesis of $ZnFe_2O_4$ nanoparticles with tunable magnetic and sensing properties, Langmuir 29 (2013) 8997-9003. https://doi.org/10.1021/la401627x.
51. X. Zhou, J.Y. Liu, C. Wang, P. Sun, X.L. Hu, X.W. Li, K. Shimanoe, N. Yamazoe, G.Y. Lu, Highly sensitive acetone gas sensor based on porous $ZnFe_2O_4$ nanospheres, Sens. Actuators, B 2015; 206: 577-583. https://doi.org/10.1016/j.snb.2014.09.080.
52. C.J. Dong, X. Liu, X.C. Xiao, S.F. Du, Y.D. Wang, Monodisperse $ZnFe_2O_4$ nanospheres synthesized by a nonaqueous route for a highly selective low-ppm-level toluene gas sensor, Sens. Actuators, B 239 (2017) 1231-1236. https://doi.org/10.1016/j.snb.2016.09.122.
53. X. Zhou, X.W. Li, H.B. Sun, P. Sun, X.S. Liang, F.M. Liu, X.L. Hu, G.Y. Lu, Nanosheet-assembled $ZnFe_2O_4$ hollow microspheres for high-sensitive acetone sensor, ACS Appl. Mater. Interfaces 7 (2015) 15414-15421. https://doi.org/10.1021/acsami.5b03537.
54. F.D. Qu, W.N. Shang, T.J. Thomas, S.P. Ruan, M.H. Yang, Self-template derived $ZnFe_2O_4$ double-shell microspheres for chemresistive gas sensing, Sens. Actuators, B 265 (2018) 625-31. https://doi.org/10.1016/j.snb.2018.03.108.
55. X.S. Niu, W.P. Du, W.M. Du, Preparation and gas sensing properties of ZnM_2O_4 (M = Fe, Co, Cr). Sens. Actuators, B 99 (2004) 405-409. https://doi.org/10.1016/j.snb.2003.12.007.
56. X.Z. Song, Y.L. Meng, Z.Q. Tan, L. Qiao, T. Huang, X.F. Wang, Concave $ZnFe_2O_4$ hollow octahedral

nanocages derived from Fe-doped MOF-5 for high-performance acetone sensing at Low-energy consumption, Inorg. Chem. 56 (2017) 13646-13650. https://doi.org/10.1021/acs.inorgchem.7b02425.

57. X.Q. Tang, X.H. Hou, L.M. Yao, S.J. Hu, X. Liu, L.Z. Xiang, Mn-doped $ZnFe_2O_4$ nanoparticles with enhanced performances as anode materials for lithium ion batteries, Mater. Res. Bull. 57 (2014) 127-134. https://doi.org/10.1016/j.materresbull.2014.05.038.
58. Quinzeni, V. Berbenni, D. Capsoni, M. Bini, Ca - and Al - doped $ZnFe_2O_4$ nanoparticles as possible anode materials, J. Solid State Electrochem. 22 (2018) 2013-2024. https://doi.org/10.1007/s10008-018-3901-7.
59. A. Manikandan, J. Judith Vijaya, M. Sundararajan, C. Meganathan, L. John Kennedy, M. Bououdina, Optical and magnetic properties of Mg-doped $ZnFe_2O_4$ nanoparticles prepared by rapid microwave combustion method, Superlattices Microstruct. 64 (2013) 118-131. https://doi.org/10.1016/j.spmi.2013.09.021.
60. Y.Y. Zhang, Y. Chen, Q.W. Kou, Z. Wang, D.L. Han, Y.T. Sun, J.H. Yang, Y. Liu, L.L. Yang, Effects of Nd concentration on structural and magnetic properties of $ZnFe_2O_4$ nanoparticles, J. Mater. Sci.: Mater. Electron. 29 (2018) 3665-3671. https://doi.org/10.1007/s10854-017-8297-0.
61. M. Maletin, E.G. Moshopoulou, A.G. Kontos, E. Devlin, A. Delimitis, V.T. Zaspalis, L. Nalbandian, V.V. Srdic, Synthesis and structural characterization of In-doped $ZnFe_2O_4$ nanoparticles, J. Eur. Ceram. Soc. 27 (2007) 4391-4394. https://doi.org/10.1016/j.jeurceramsoc.2007.02.165.
62. A. Singh, S. Singh, B.D. Joshi, A. Shukla, B.C. Yadav, P. Tandon, Synthesis, characterization, magnetic properties and gas sensing applications of $Zn_xCu_{1-x}Fe_2O_4$ ($0.0 \leq x \leq 0.8$) nanocomposites, Mater. Sci. Semicond. Process. 27 (2014) 934-949. https://doi.org/10.1016/j.mssp.2014.08.029.
63. M.C. Daniel, D. Astruc, Gold Nanoparticles: assembly, supramolecular chemistry, quantum-size-related properties, and applications toward biology, catalysis, and nanotechnology, Chem. Rev. 104 (2004) 293-246. https://doi.org/10.1021/cr030698+.
64. C. Zhang, Q.D. Wu, B.B. Zheng, J.J. You, Y.F. Luo, Synthesis and acetone gas sensing properties of Ag activated hollow sphere structured $ZnFe_2O_4$, Ceram. Int. 44 (2018) 20700-20707. https://doi.org/10.1016/j.ceramint.2018.08.064.
65. J.T. Wu, D.J. Gao, T. Sun, J. Bi, Y. Zhao, Z.L. Ning, G.Y. Fan, Z.X. Xie, Highly selective gas sensing properties of partially inversed spinel zinc ferrite towards H_2S, Sens. Actuators, B 235 (2016) 258-262. https://doi.org/10.1016/j.snb.2016.05.083.
66. P.K. Basu, S.K. Jana, H. Saha, S. Basu, Low temperature methane sensing by electrochemically grown and surface modified ZnO thin films, Sens. Actuators, B 135 (2008) 81-88. https://doi.org/10.1016/j.snb.2008.07.021.
67. Y. Yan, P. Nizamidin, G. Turdi, N. Kari, A. Yimit, Room-temperature H_2S gas sensor based on Au-doped $ZnFe_2O_4$ yolk-shell microspheres, Anal. Sci. 33 (2017) 945-951. https://doi.org/10.2116/analsci.33.945.
68. P. Ghosh, M.R. Das, P. Mitra, Influence of particle size on H_2 and H_2S sensing characteristics of nanocrystalline zinc ferrite, Indian J. Phys. 90 (2017) 1367-1373. https://doi.org/10.1007/s12648-016-0888-8.
69. H.R. Ebrahimi, M. Parish, G.R. Amiri, B. Bahraminejad, S. Fatahian, Synthesis, characterization and gas sensitivity investigation of $Ni_{0.5}Zn_{0.5}Fe_2O_4$ nanoparticles, J. Magn. Magn. Mater. 414 (2016) 55-58. https://doi.org/10.1016/j.jmmm.2016.04.043.
70. K. Mukherjee, S.B. Majumder, Synthesis of embedded and isolated $Mg_{0.5}Zn_{0.5}Fe_2O_4$ nano-tubes and investigation on their anomalous gas sensing characteristics, Sens. Actuators, B 177 (2013) 55-63. https://doi.org/10.1016/j.snb.2012.10.108.
71. K. Mukherjee, S.B. Majumder, Hydrogen sensing characteristics of nano-crystalline $Mg_{0.5}Zn_{0.5}Fe_2O_4$ thin film: Effect of film thickness and operating temperature, Int. J. Hydrogen Energy 39 (2014) 1185-1191. https://doi.org/10.1016/j.ijhydene.2013.10.158.

72. C. Mukherjee, R. Mondal, S. Dey, S. Kumar, J. Das, Nanocrystalline CopperNickelZinc Ferrite: Efficient sensing materials for ethanol and acetone at room temperature, IEEE Sens. J. 17 (2017) 2662-2669. https://doi.org/10.1109/JSEN.2017.2684838.
73. K. Xiong, K.Z. Wang, L. Chen, X.Q. Wang, Q.B. Fan, J. Courtois, Y.L. Liu, X.G. Tuo, M.H. Yan, Heterostructured $ZnFe_2O_4/Fe_2TiO_5/TiO_2$ composite nanotube arrays with an improved photocatalysis degradation efficiency under simulated sunlight irradiation, Nano-Micro Lett. 10 (2018) 17. https://doi.org/10.1007/s40820-017-0169-x.
74. P.F. Hu, C.C. Chen, J.W. Song, Z.H. Tang, Efficient visible-light photocatalysis of ZIF-derived mesoporous $ZnFe_2O_4$/ZnO nanocomposite prepared by a two-step calcination method, Mater. Sci. Semicond. Process. 77 (2018) 40-49. https://doi.org/10.1016/j.mssp.2018.01.012.
75. Y.W. Li, N. Luo, G. Sun, B. Zhang, G.Z. Ma, H.H. Jin, Y. Wang, J.L. Cao, Z.Y. Zhang, Facile synthesis of $ZnFe_2O_4/\alpha$-Fe_2O_3 porous microrods with enhanced TEA-sensing performance, J. Alloys Compd. 737 (2018) 255-262. https://doi.org/10.1016/j.jallcom.2017.12.068.
76. S.M. Li, L.X. Zhang, M.Y. Zhu, G.J. Ji, L.X. Zhao, J. Yin, L.J. Bie, Acetone sensing of ZnO nanosheets synthesized using room-temperature precipitation, Sens. Actuators, B 249 (2017) 611-623. https://doi.org/10.1016/j.snb.2017.04.007.
77. S. Narasimman, L. Balakrishnan, S.R..Meher, R. Sivacoumar, Z.C. Alex, Influence of surface functionalization on the gas sensing characteristics of ZnO nanorhombuses. J. Alloys Compd. 706 (2017) 186-197. https://doi.org/10.1016/j.jallcom.2017.02.160.
78. S.R. Wang, J.X. Zhang, J.D. Yang, X.L. Gao, H.X. Zhang, Y.S. Wang, Z.Y. Zhu, Spinel $ZnFe_2O_4$ nanoparticle-decorated rod-like ZnO nanoheterostructures for enhanced gas sensing performances, RSC Adv. 5 (2015) 10048-10057. https://doi.org/10.1039/c4ra14033h.
79. J. Ma, Y.X. Cai, X.W. Li, S.T. Yao, Y. Liu, F.M. Liu, G.Y. Lu, Synthesis of hierarchical ZnO/$ZnFe_2O_4$ nanoforests with enhanced gas-sensing performance toward ethanol, CrystEngComm 17 (2015) 8683-8688. https://doi.org/10.1039/c5ce01919b.
80. C. Liu, B.Q. Wang, T.S. Wang, J.Y. Liu, P. Sun, X.H. Chuai, G.Y. Lu, Enhanced gas sensing characteristics of the flower-like $ZnFe_2O_4$/ZnO microstructures, Sens. Actuators, B 248 (2017) 902-909. https://doi.org/10.1016/j.snb.2017.01.133.
81. M.H. Oh, T.Y. Yu, S.H. Yu, B.K. Lim, K.T. Ko, M.G. Willinger, D.H. Seo, B.H. Kim, M.G. Cho, A.H. Park, K. Kang, Y.E. Sung, N. Pina, T. Hyeon, Galvanic replacement reactions in metal oxide nanocrystals, Science 340 (2013) 964-968. https://doi.org/10.1126/science.1234751.
82. X.J. Wang, J. Feng, Y.C. Bai, Q. Zhang, Y.D. Yin, Synthesis, properties, and applications of hollow micro-/nanostructures, Chem. Rev. 116 (2016) 10983-11060. https://doi.org/10.1021/acs.chemrev.5b00731.
83. L. Yu, H.B. Wu, X.W. Lou, Self-templated formation of hollow structures for electrochemical energy applications, Accounts Chem. Res. 50 (2017) 293-301. https://doi.org/10.1016/j.jallcom.2018.12.348.
84. R. Zhang, T. Zhang, T.T. Zhou, Z. Lou, J.N. Deng, L.L. Wang, Fast and real-time acetone gas sensor using hybrid $ZnFe_2O_4$/ZnO hollow spheres, RSC Adv. 6 (2016) 66738-66744. https://doi.org/10.1039/c6ra12201a.
85. X. Wang, S.W. Zhang, M.H. Shao, J.Z. Huang, X.L. Deng, P.Y. Hou, X.J. Xu, Fabrication of ZnO/$ZnFe_2O_4$ hollow nanocages through metal organic frameworks route with enhanced gas sensing properties, Sens. Actuators, B 251 (2017) 27-33. https://doi.org/10.1016/j.snb.2017.04.114.
86. X.Z. Song, L. Qiao, K.M. Sun, Z.Q. Tan, W. Ma, X.L. Kang, F.F. Sun, T. Huang, X.F. Wang, Triple-shelled ZnO/$ZnFe_2O_4$ heterojunctional hollow microspheres derived from Prussian Blue analogue as high-performance acetone sensors, Sens. Actuators, B 256 (2018) 374-382. https://doi.org/10.1016/j.snb.2017.10.081.

87. W. Gao, R. Huang, Thermomechanics of monolayer graphene: Rippling, thermal expansion and elasticity, J. Mech. Phys. Solids (2014) 66 42-58. https://doi.org/10.1016/j.jmps.2014.01.011.
88. M.V. Jacob, D. Taguchi, M. Iwamoto, K. Bazaka, R.S. Rawat, Resistive switching in graphene-organic device: Charge transport properties of graphene-organic device through electric field induced optical second harmonic generation and charge modulation spectroscopy, Carbon 112 (2017) 111-116. https://doi.org/10.1016/j.carbon.2016.11.005.
89. C. Lee, X. Wei, J.W. Kysar, J. Hone, Measurement of the elastic properties and intrinsic strength of monolayer graphene, Science 321 (2008) 385-388. https://doi.org/10.1126/science.1157996.
90. S.M. Hafiz, R. Ritikos, T.J. Whitcher, N.M. Razib, D. Bien, N. Chanlek, H. Nakajima, T. Saisopa, P. Songsiriritthigul, N.M. Huang, S.A. Rahman, A practical carbon dioxide gas sensor using room-temperature hydrogen plasma reduced graphene oxide, Sens. Actuators, B 193 (2014) 692-700. https://doi.org/10.1016/j.snb.2013.12.017.
91. Y. Seekaew, D. Phokharatkul, A. Wisitsoraat, C. Wongchoosuk, Highly sensitive and selective room-temperature NO_2 gas sensor based on bilayer transferred chemical vapor deposited graphene, Appl. Surf. Sci. 404 (2017) 357-363. https://doi.org/10.1016/j.apsusc.2017.01.286.
92. J. Liu, S. Li, B. Zhang, Y.L. Wang, Y. Gao, X.S. Liang, Y. Wang, G.Y. Lu, Flower-like In_2O_3 modified by reduced graphene oxide sheets serving as a highly sensitive gas sensor for trace NO_2 detection, J. Colloid Interf. Sci. 504 (2017) 206-213. https://doi.org/10.1016/j.jcis.2017.05.053.
93. B. Zhang, J. Liu, X.B. Cui, Y.L. Wang, Y. Gao, P. Sun, F.M. Liu,K. Shimanoe, N. Yamazoe, G.Y. Lu, Enhanced gas sensing properties to acetone vapor achieved by α-Fe_2O_3 particles ameliorated with reduced graphene oxide sheets, Sens. Actuators, B 241 (2017) 904-914. https://doi.org/10.1016/j.snb.2016.11.023.
94. D.J. Sun,Y.F. Luo, M. Debliquy, C. Zhang, Graphene-enhanced metal oxide gas sensors at room temperature: a review, Beilstein J. Nanotechnol. 9 (2018) 2832-2844. https://doi.org/10.3762/bjnano.9.264.
95. P. Fei, Q. Wang, M. Zhong, B. Su, Preparation and adsorption properties of enhanced magnetic zinc ferrite-reduced graphene oxide nanocomposites via a facile one-pot solvothermal method, J. Alloys Compd. 685 (2016) 411-417. https://doi.org/10.1016/j.jallcom.2016.05.279.
96. F. Liu, X.F. Chu, Y.P. Dong, W.B. Zhang, W.Q. Sun, L.M. Shen, Acetone gas sensors based on graphene-$ZnFe_2O_4$ composite prepared by solvothermal method, Sens. Actuators, B 188 (2013) 469-474. https://doi.org/10.1016/j.snb.2013.06.065.
97. W. Hong, L.Z. Li, R.N. Xue, X.Y. Xu, H. Wang, J.K. Zhou, H.L. Zhao, Y.H. Song, Y. Liu, One-pot hydrothermal synthesis of Zinc ferrite/reduced graphene oxide as an efficient electrocatalyst for oxygen reduction reaction, J. Colloid Interf. Sci. 485 (2017) 175-182. https://doi.org/10.1016/j.jcis.2016.04.035.
98. Z.W. Yang, Y.Z. Wan, G.Y. Xiong, D.Y. Li, Q.P. Li, C.Y. Ma, R.S. Guo, H.L. Luo, Facile synthesis of $ZnFe_2O_4$/reduced graphene oxide nanohybrids for enhanced microwave absorption properties, Mater. Res. Bull. 61 (2015) 292-297. https://doi.org/10.1016/j.materresbull.2014.10.004.
99. X. Ma, X.Y. Zhou, Y. Gong, N. Han, H.D. Liu, Y.F. Chen, MOF-derived hierarchical ZnO/$ZnFe_2O_4$ hollow cubes for enhanced acetone gas-sensing performance, RSC Adv. 7 (2017) 34609-34617. https://doi.org/10.1039/c7ra04437b.
100. Y.W. Li, N. Luo, G. Sun, B. Zhang, G.Z. Ma, H.H. Jin, Y. Wang, J.L. Cao, Z.Y. Zhang, Facile synthesis of $ZnFe_2O_4$/α-Fe_2O_3 porous microrods with enhanced TEA-sensing performance, J. Alloys Compd. 737 (2018) 255-262. https://doi.org/10.1016/j.jallcom.2017.12.068.
101. S.D. Raut, V.V. Awasarmol, B.G. Ghule, S.F. Shaikh, S.K. Gore, R.P. Sharma, P.P. Pawar, R.S. Mane, Gamma-irradiation induced zinc ferrites and their enhanced room-temperature ammonia gas sensing properties, Mater. Res. Express 5 (2018) 035702. https://doi.org/10.1088/2053-1591/aab3eb.

102. A. Sutka, G. Mezinskis, A. Lusis, D. Jakovlevs, Influence of iron non-stoichiometry on spinel zinc ferrite gas sensing properties, Sens. Actuators, B 171-172 (2012) 204-209. https://doi.org/10.1016/j.snb.2012.03.012.

Figures Captions

Fig. 1 The crystal structure of $ZnFe_2O_4$ (A=Zn^{2+}, B=Fe^{3+}), Zn^{2+} in the space between tetrahedron, Fe^{3+} in the octahedron gap. Reprinted with permission from Ref. [27]. Copyright 2018: Elsevier.

Fig. 2 Schematic of acetone sensing mechanism of $ZnFe_2O_4$ gas sensor.

Fig. 3 Under the condition of 200°C, (a) the real-time response curves of acetone ZnO and $ZnFe_2O_4$ sensor, (b) real-time resistance curves of $ZnFe_2O_4$ sensor. Reprinted with permission from Ref. [36]. Copyright 2015: Elsevier.

Fig. 4 (a-b) SEM images of $ZnFe_2O_4$ nanorods, (c-e) TEM images of $ZnFe_2O_4$ nanorods, (f) Response of $ZnFe_2O_4$ nanorod sensors to 10-500 ppm acetone and ethanol at 260°C, (g) Response curves of $ZnFe_2O_4$-nanoparticles gas sensor to 10-100 ppm acetone at 260°C. Adapted with permission from Ref. [43]. Copyright 2017: Elsevier.

Fig. 5 TEM images of $ZnFe_2O_4$ tubes obtained using sol precursors of: (a) 0.15 M, (b1) 0.25 M, and (c) 0.4 M. (b2) The HRTEM image of partial wall of a single tube in (b1), and the inset is the enlargement of the marked square. Reprinted with permission from Ref. [45]. Copyright 2007: Elsevier.

Fig. 6 Schematic of the gas sensing mechanism of ZnO/$ZnFe_2O_4$ sensor to acetone, based on the dynamic response curve of the pure ZnO, pure $ZnFe_2O_4$ and ZnO/$ZnFe_2O_4$ complex sensor to acetone of 5-700 ppm. Reprinted with permission from Ref. [47]. Copyright 2015: American Chemical Society.

Fig. 7 Schematic illustration of acetone sensing mechanism for hollow $ZnFe_2O_4$ microspheres (a) in air (b) in acetone. Reprinted with permission from Ref. [53]. Copyright 2015: American Chemical Society.

Fig. 8 TEM images of (a) pure $ZnFe_2O_4$ (b) 0.25 wt% Ag-$ZnFe_2O_4$. Dynamic response-recovery curves to acetone vapor of Ag-$ZnFe_2O_4$ sensors at 175°C: (c) 0.8-500 ppm (d) 0.8-10 ppm. Dynamic response-recovery curves of (e) 0.25 wt% Ag-$ZnFe_2O_4$ sensor and (f) pure $ZnFe_2O_4$ sensor to 100 ppm acetone vapor at 175°C. Adapted with permission from Ref. [64]. Copyright 2018: Elsevier.

Fig. 9 Schematic of (a and c) gas sensing mechanisms and (b) energy band structures of $ZnFe_2O_4$/ZnO based sensor. Reprinted with permission from Ref. [84]. Copyright 2016: Royal Society of Chemistry.

Fig. 10 Structural characterization of ZZFO TSHMs: (a,b) FESEM and (c,d) TEM images. Adapted with permission from Ref. [86]. Copyright 2018: Elsevier.

Fig. 11 The synthesis mechanism of $ZnFe_2O_4$-rGO obtaining from Zn^{2+}, Fe^{3+} and GO. Reprinted with permission from Ref. [95]. Copyright 2016: Elsevier.

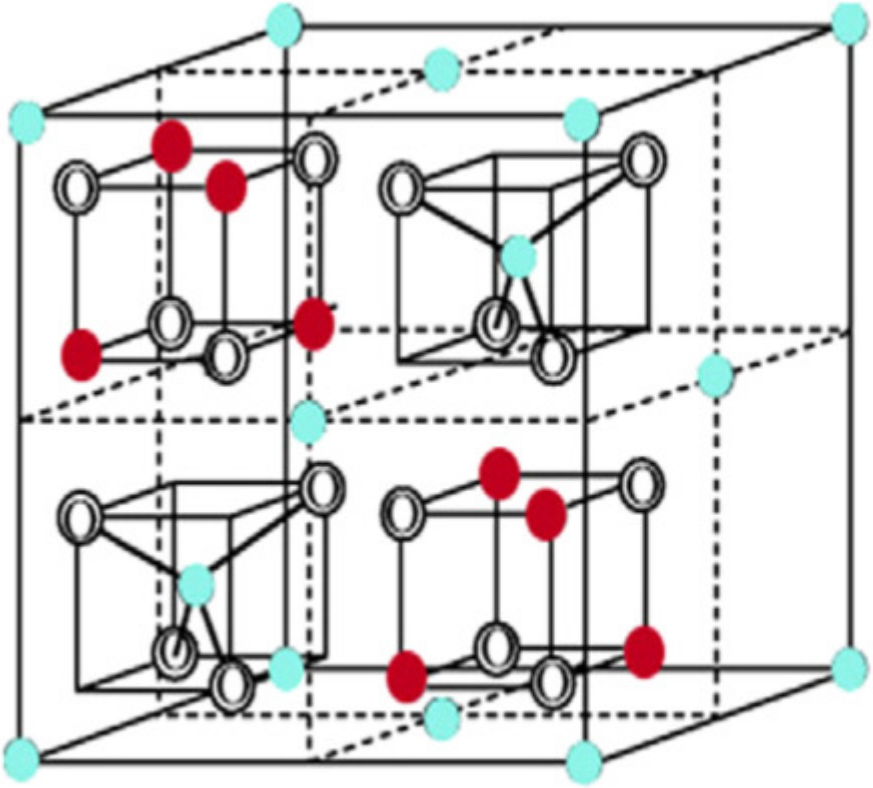

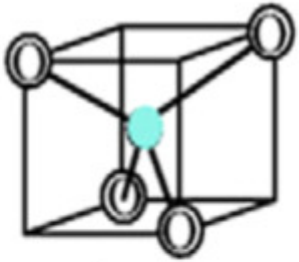

A site

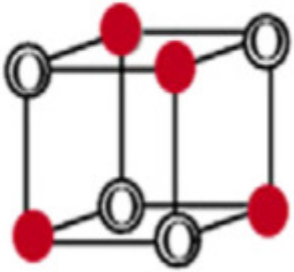

B site

Octahedral sites Tetrahedral sites Oxigen

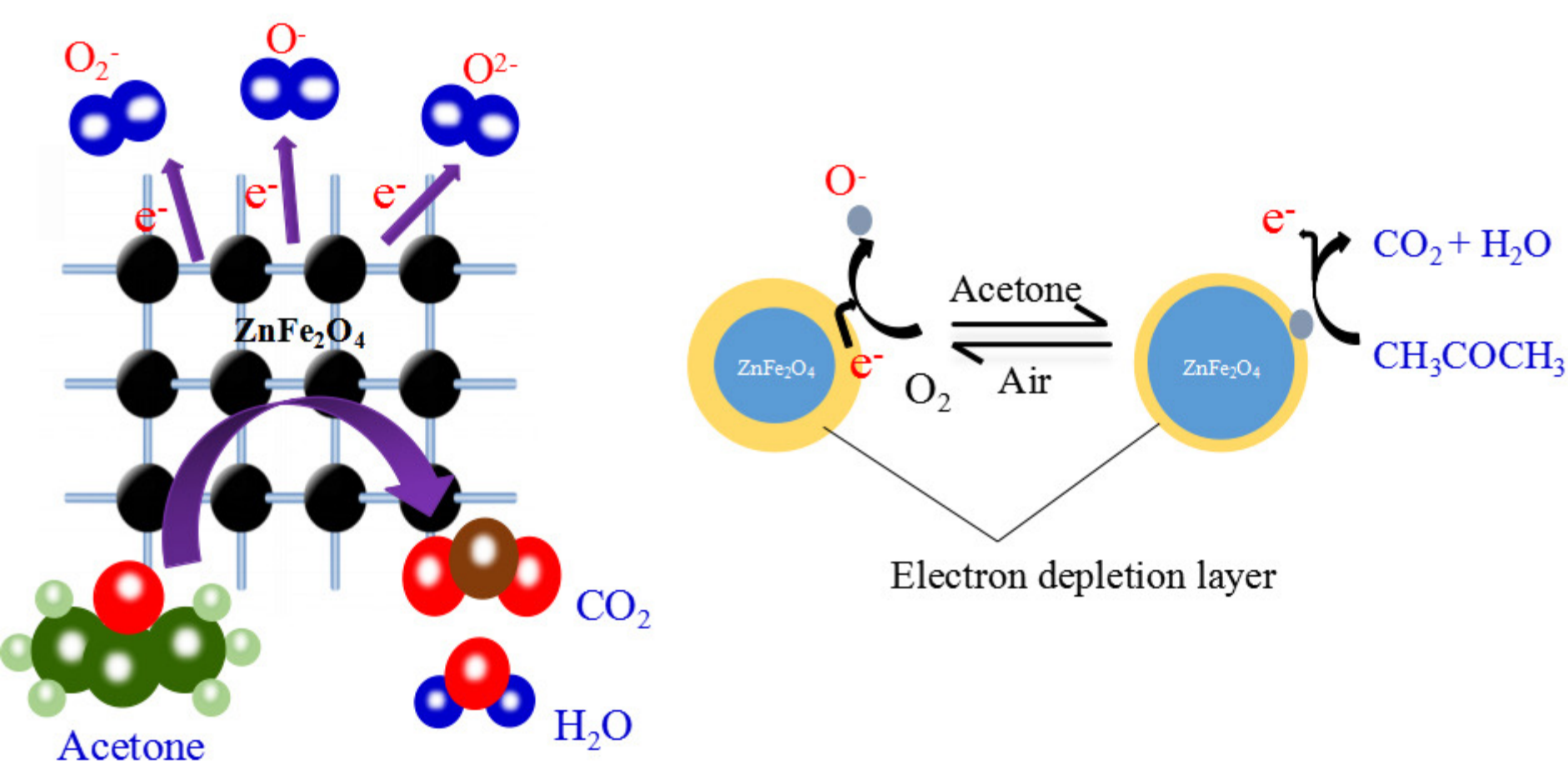
O_2^-
O^-
O^{2-}
e-
e-
e-
$ZnFe_2O_4$
CO_2
H_2O
Acetone
O^-
e-
$ZnFe_2O_4$
O_2
Acetone
Air
$ZnFe_2O_4$
e-
$CO_2 + H_2O$
CH_3COCH_3
Electron depletion layer

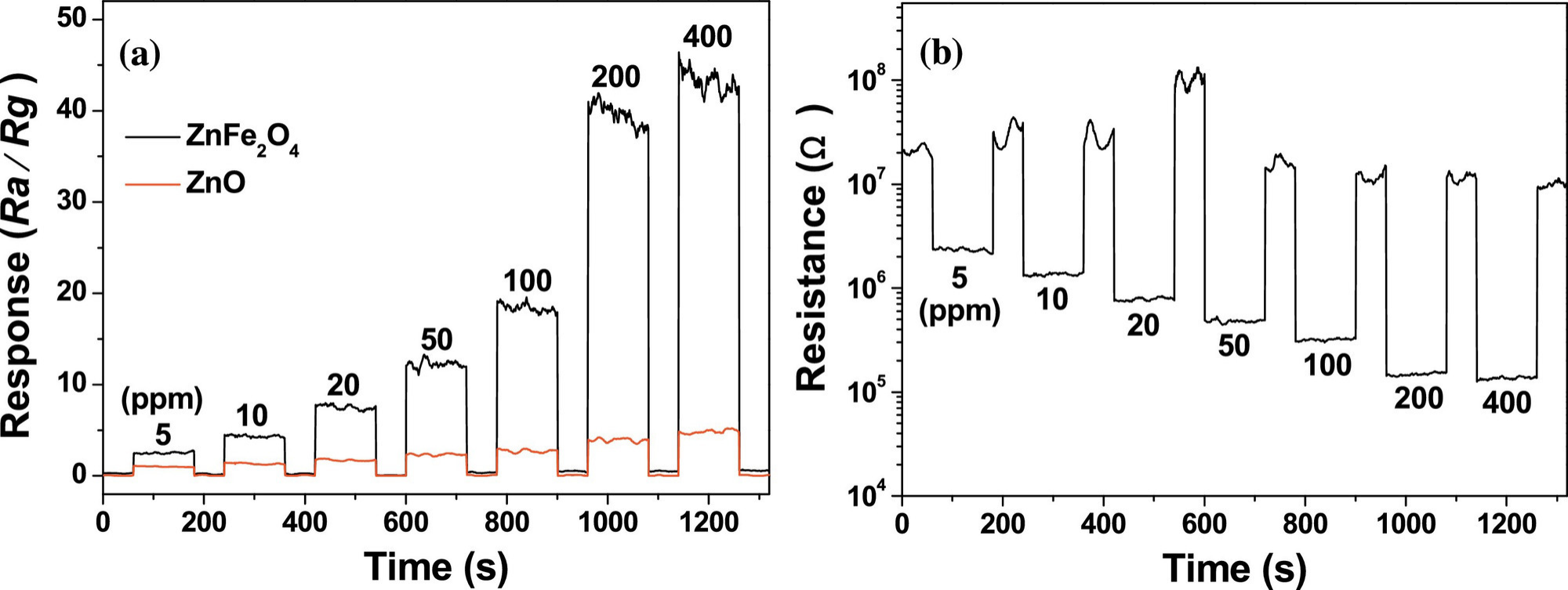
(a)
ZnFe2O4
ZnO
(ppm)
5
10
20
50
100
200
400
Response (Ra / Rg)
Time (s)
(b)
Resistance (Ω)
Time (s)

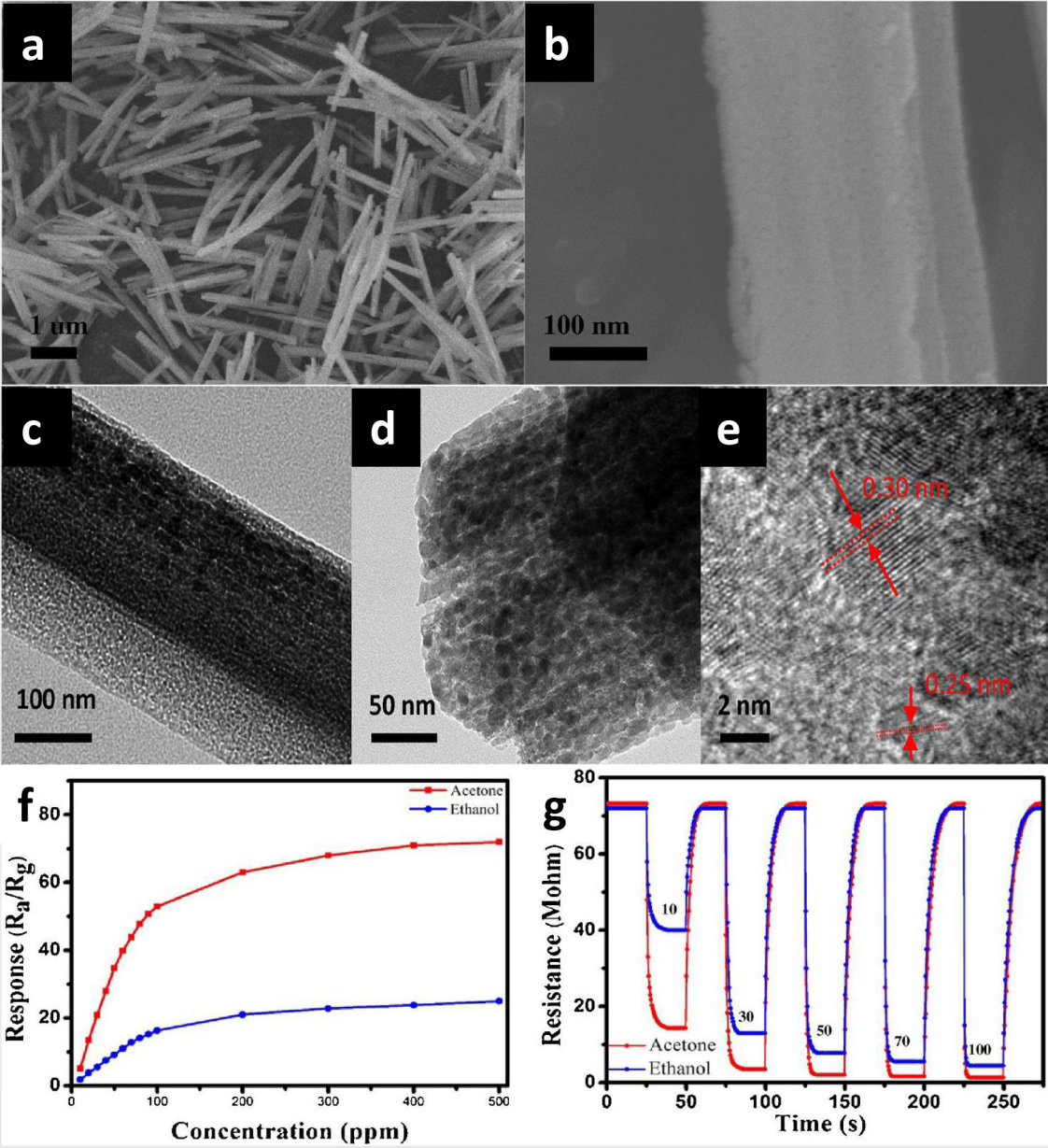
a
1 um
b
100 nm
c
100 nm
d
50 nm
e
0.30 nm
0.25 nm
2 nm
f
Acetone
Ethanol
Response (R_a/R_g)
Concentration (ppm)
g
Resistance (Mohm)
Time (s)
10
30
50
70
100
Acetone
Ethanol

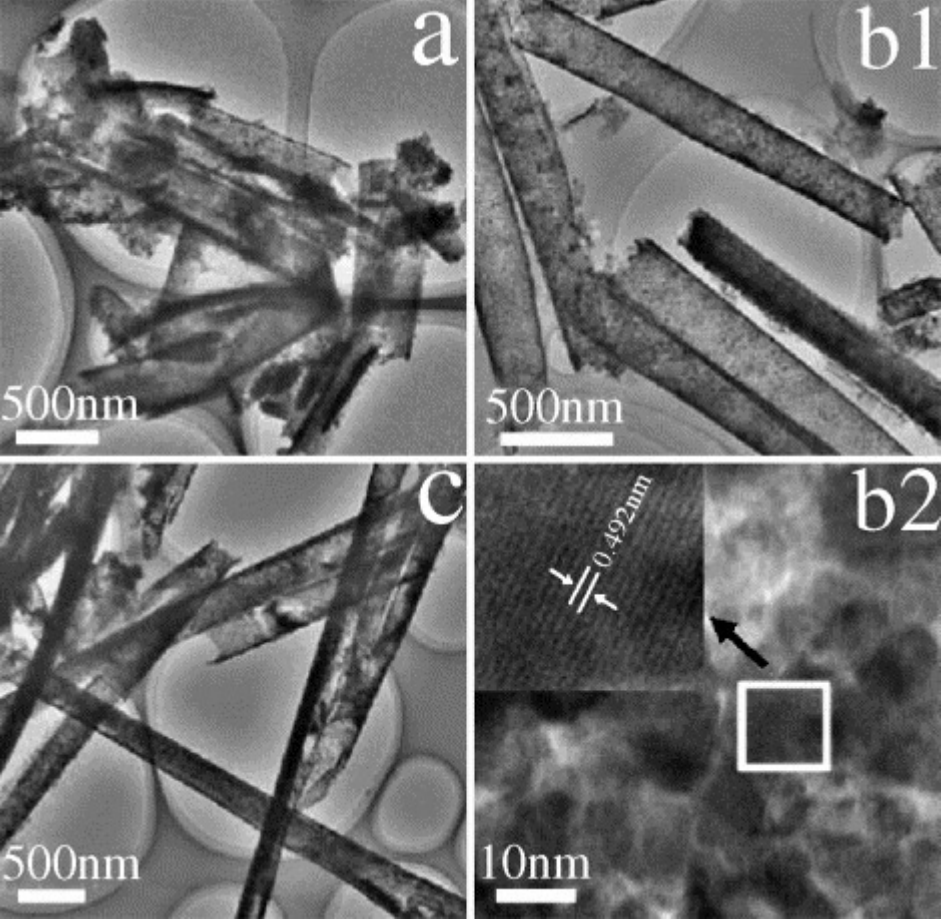
a
500nm
b1
500nm
c
500nm
b2
0.492nm
10nm

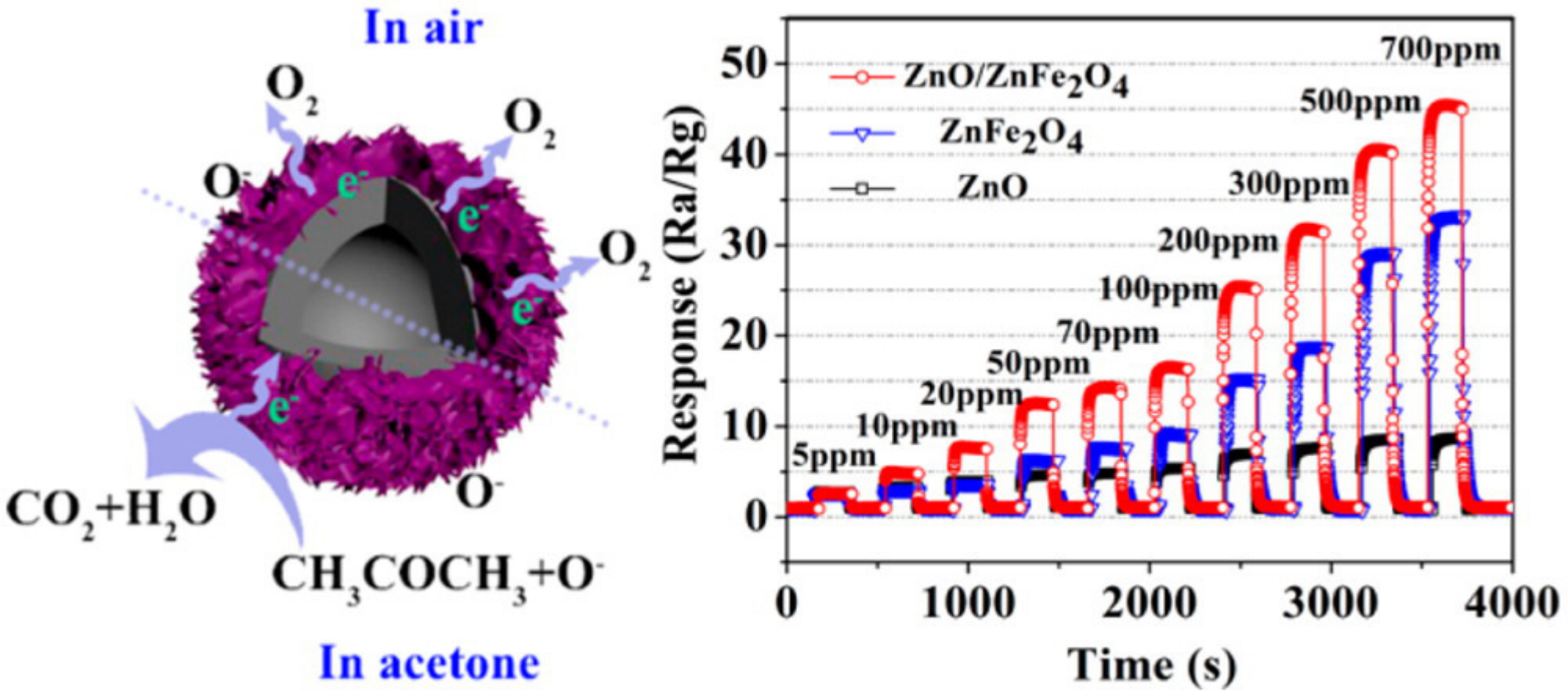
In air
O2
O2
O2
O-
e-
e-
e-
e-
O-
CO2+H2O
CH3COCH3+O-
In acetone
ZnO/ZnFe2O4
ZnFe2O4
ZnO
5ppm
10ppm
20ppm
50ppm
70ppm
100ppm
200ppm
300ppm
500ppm
700ppm
Response (Ra/Rg)
Time (s)
0
10
20
30
40
50
0
1000
2000
3000
4000

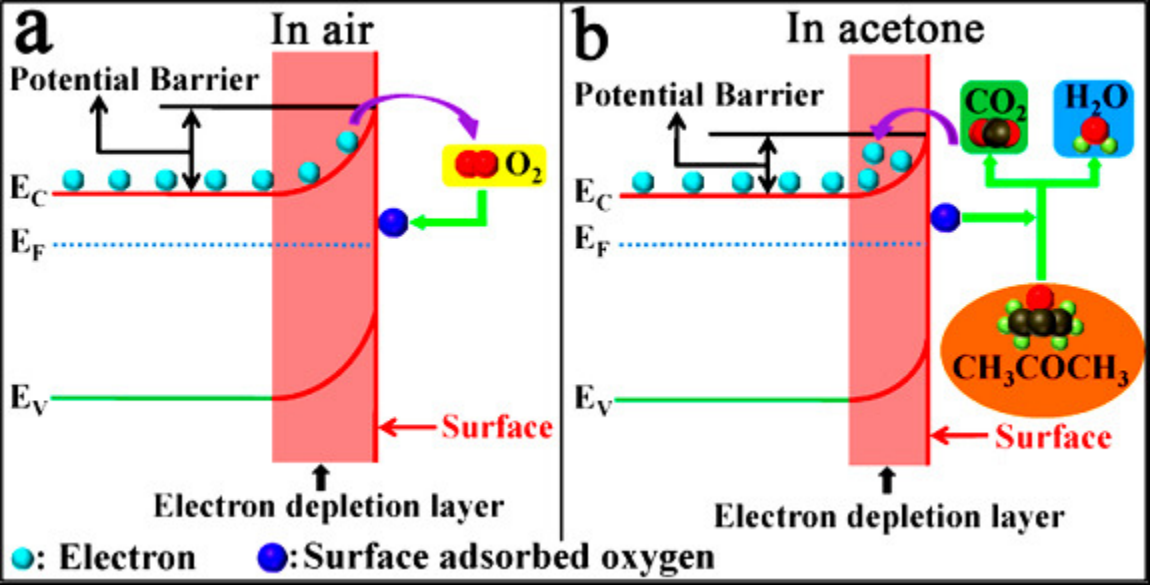
a
In air
Potential Barrier
E_C
E_F
E_V
O_2
Surface
Electron depletion layer
b
In acetone
Potential Barrier
E_C
E_F
E_V
CO_2
H_2O
CH_3COCH_3
Surface
Electron depletion layer
: Electron
:Surface adsorbed oxygen

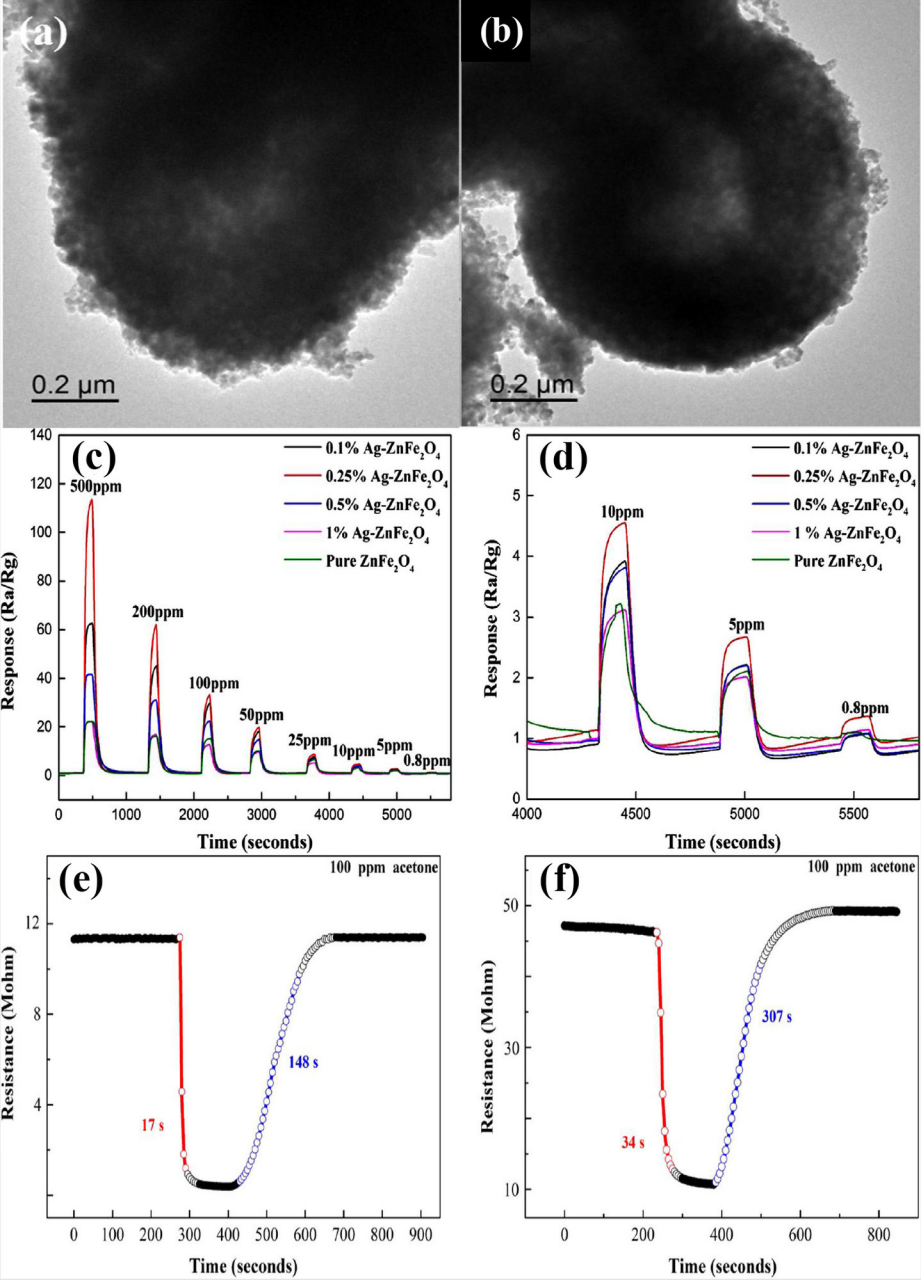
(a)
0.2 μm
(b)
0.2 μm
(c)
0.1% Ag-ZnFe2O4
0.25% Ag-ZnFe2O4
0.5% Ag-ZnFe2O4
1% Ag-ZnFe2O4
Pure ZnFe2O4
500ppm
200ppm
100ppm
50ppm
25ppm
10ppm
5ppm
0.8ppm
Response (Ra/Rg)
Time (seconds)
(d)
0.1% Ag-ZnFe2O4
0.25% Ag-ZnFe2O4
0.5% Ag-ZnFe2O4
1 % Ag-ZnFe2O4
Pure ZnFe2O4
10ppm
5ppm
0.8ppm
Response (Ra/Rg)
Time (seconds)
(e)
100 ppm acetone
17 s
148 s
Resistance (Mohm)
Time (seconds)
(f)
100 ppm acetone
34 s
307 s
Resistance (Mohm)
Time (seconds)

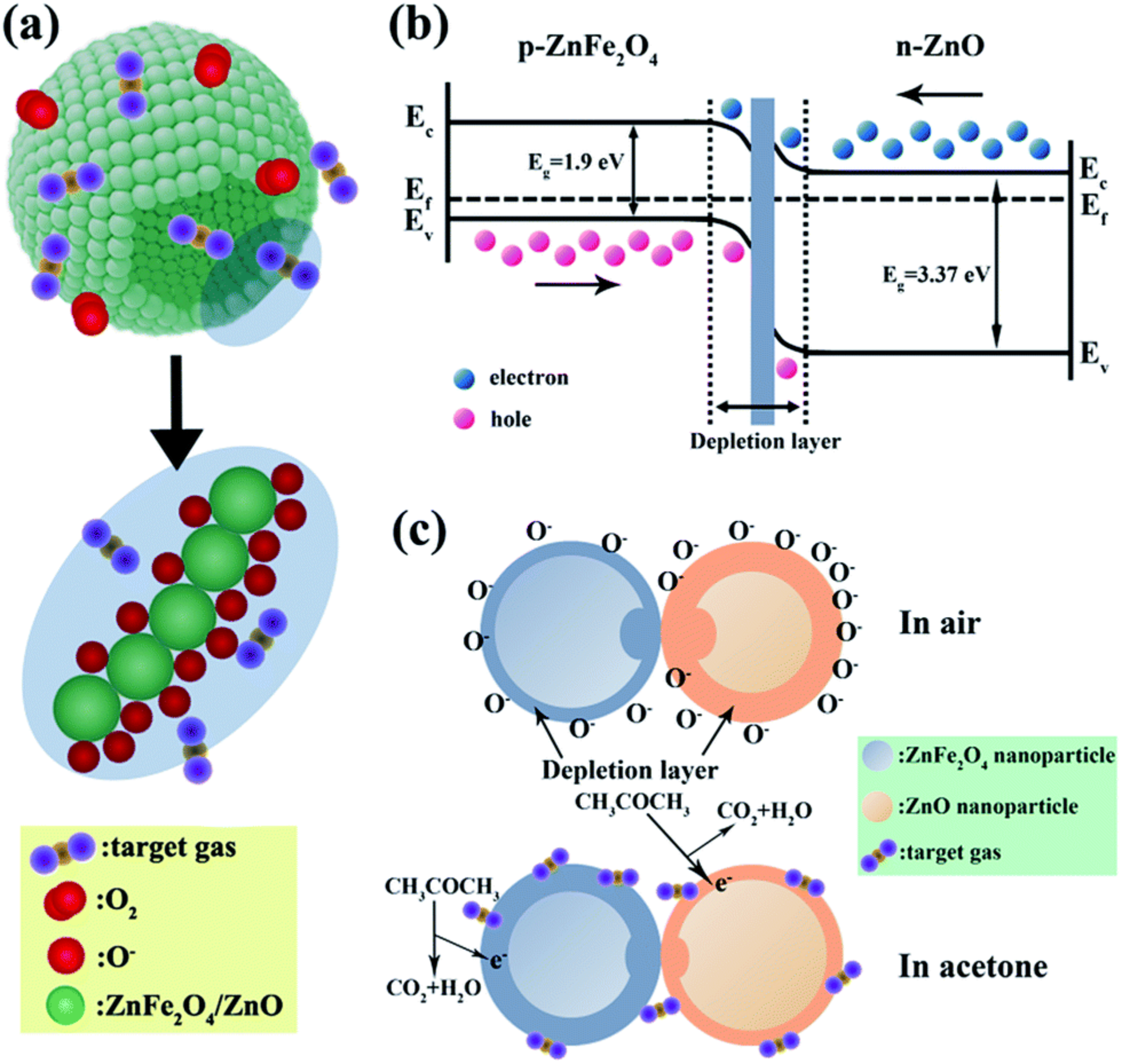
(a)
(b)
p-ZnFe2O4
n-ZnO
Ec
Ef
Ev
Eg=1.9 eV
Eg=3.37 eV
electron
hole
Depletion layer
(c)
O-
In air
Depletion layer
:ZnFe2O4 nanoparticle
:ZnO nanoparticle
:target gas
CH3COCH3
CO2+H2O
e-
In acetone
:target gas
:O2
:O-
:ZnFe2O4/ZnO

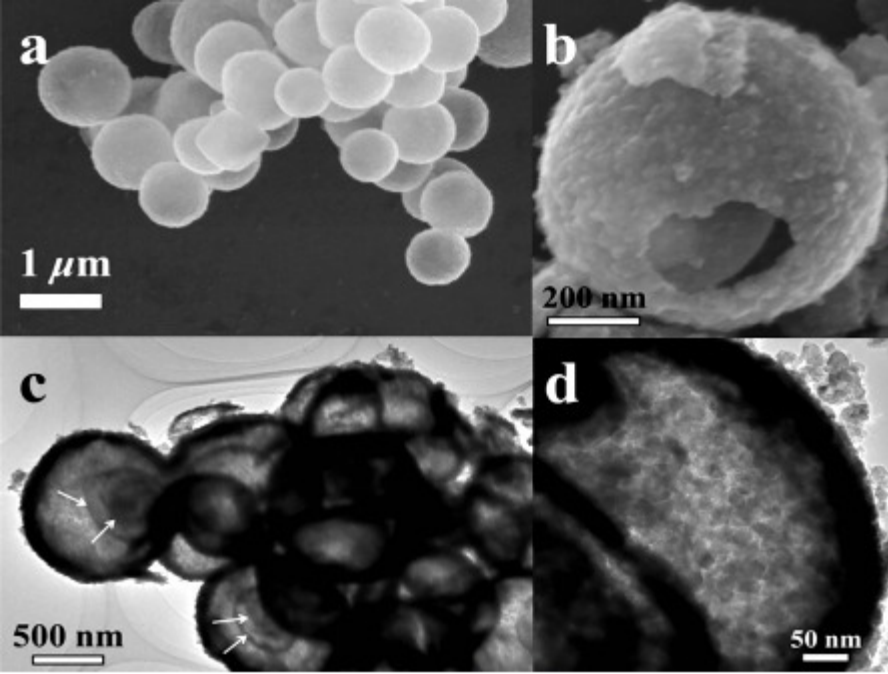
a
1 μm
b
200 nm
c
500 nm
d
50 nm

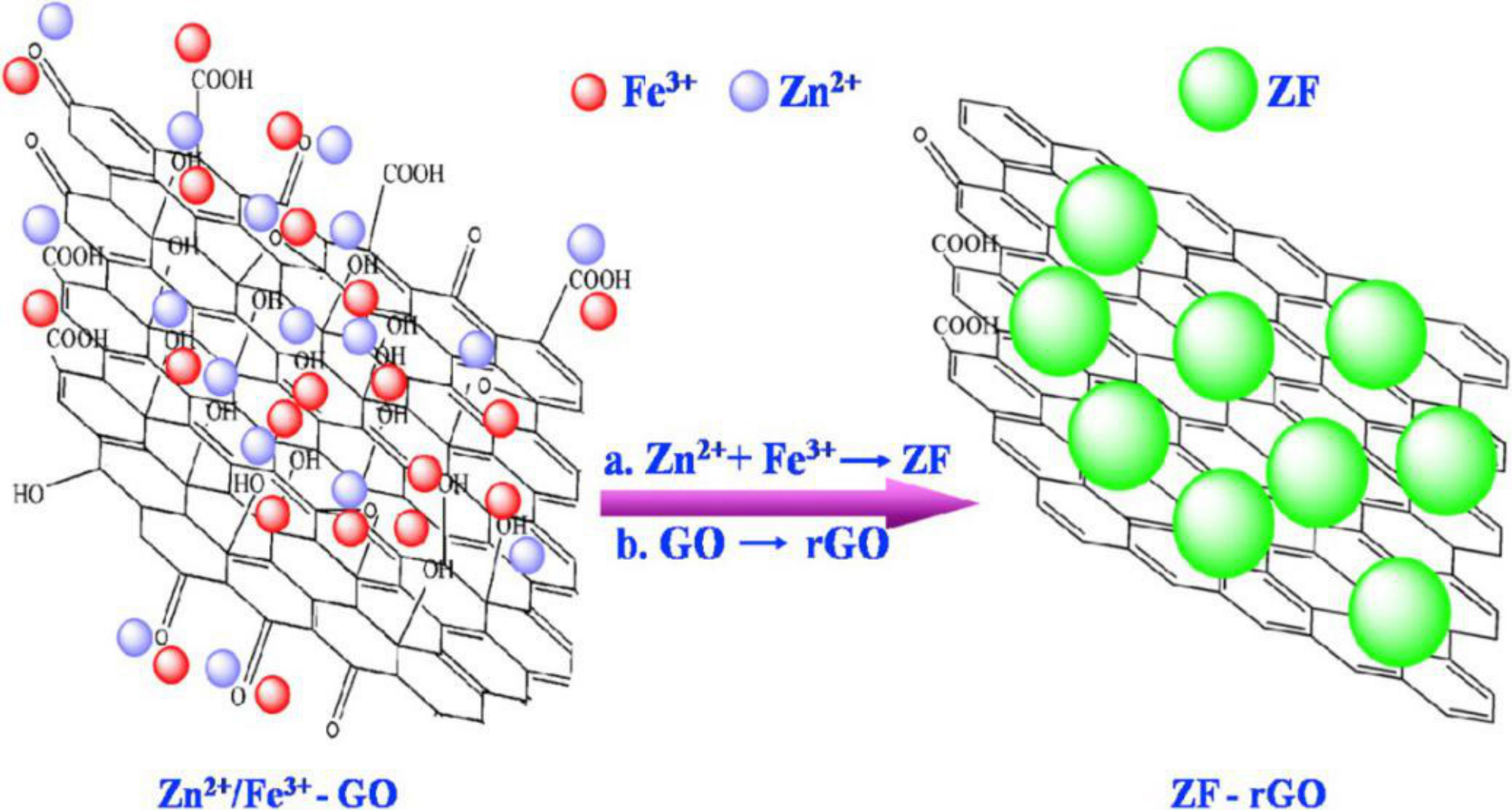
Fe3+
Zn2+
ZF
COOH
OH
HO
a. Zn2+ + Fe3+ → ZF
b. GO → rGO
Zn2+/Fe3+ - GO
ZF - rGO

Table 1 Effect of heat treatment parameters on $ZnFe_2O_4$ microstructure

Materials	Annealing Temperature	Heating rate	Morphology	Structure information		
				grain size(nm)	specific surface area ($m^2\ g^{-1}$)	pore size (nm)
$ZnFe_2O_4$	350ºC	1ºC/min	Double shell	23	108.3	14.17
	350ºC	20ºC/min	Core-shell	18	67.8	10.51
	350ºC	—	Solid microsphere	15	43.9	7.68

Note: — represented directly to heat treatment temperature 350ºC, no heating process. Source: Data extracted from Ref. [54].

Table 2 Different morphologies of $ZnFe_2O_4$ and their partial sensing properties (detecting acetone)

Materials	Morphology	Gas sensing performance			Ref.
		Conc. (ppm)	optimum operating temperature(°C)	Response(S)	
$ZnFe_2O_4$	nanoparticle	50	270	4.20	[55]
$ZnFe_2O_4$	nanorod	100	260	52.80	[43]
$ZnFe_2O_4$	nanotube	10	300	1.36	[45]
$ZnFe_2O_4$	nanosheet	10	250	5.10	[47]
$ZnFe_2O_4$	porous nanosphere	0.8	200	1.50	[51]
	core-shell	20	200	13.80	[48]
$ZnFe_2O_4$	nanosheets-assembled hollow microsphere	20	215	9.80	[53]
	double shell	5	206	2.60	[54]
$ZnFe_2O_4$	nanocage(octahedron)	10	120	6.27	[56]

Note: $S = R_a / R_g$, R_a — the resistance in air, R_g — the resistance in acetone.

Table 3 Comparison of the H_2S sensing performance of gas sensors based on various $ZnFe_2O_4$

Gas sensing materials	Operating temperature	H_2S Concentration (ppm)	Definition of response	Response	Response Time (s)	Ref.
$ZnFe_2O_4$ nanoparticle	80ºC	300	$S= R_a/R_g$	64.4	23.1	[42]
$ZnFe_2O_4$ nanosheet	85ºC	5	$S= R_a/R_g$	123.0	39.0	[46]
$ZnFe_2O_4$ (reverse spinel)	260ºC	50	$S= R_a/R_g$	36.8	8.0	[65]
1.5 wt% Au-$ZnFe_2O_4$	Room temperature	200	$S= R_a/R_g$	23.0	—	[67]
2 wt% Au-$ZnFe_2O_4$	Room temperature	100	$S= R_a/R_g$	39.9	46.0	[67]
$ZnFe_2O_4$ nanocrystalline	150ºC	200	$S=(R_a-R_g)/R_a$ *100%	82.0%	40.0	[68]

Table 4 Performance of $M_xZn_{1-x}Fe_2O_4$ sensors (M=Cu, Ni, Mg)

Materials	Target gas	Operating temperature	Conc. (ppm)	Definition of response	Response	$\tau_{res.}/\tau_{rec.}$ (s)	Ref.
$Ni_{0.5}Zn_{0.5}Fe_2O_4$	acetonitrile	350ºC	80~200	$S=(V_a-V_g)/V_g$	~2.1 (200)	~8/35 (200)	[69]
$Mg_{0.5}Zn_{0.5}Fe_2O_4$ nanotube	hydrogen	350ºC	10~1660	$S=(R_g-R_a)/R_g*100\%$	66% (1660)	~125/200 (1660)	[70]
$Mg_{0.5}Zn_{0.5}Fe_2O_4$ thin film (spin coating 15 times)	hydrogen	250ºC	20~1660	$S=(R_a-R_g)/R_a*100\%$	14~76%	~280/215(20) ~32/160(1660)	[71]
$Mg_{0.5}Zn_{0.5}Fe_2O_4$ thin film (spin coating 30 times)			50~1660		31~76%	~70/120(50) ~28/200(1660)	[71]
$Cu_{0.5}Ni_{0.25}Zn_{0.25}Fe_2O_4$	acetone	room temperature	500	$S=(R_a-R_g)/R_a*100\%$	77%	10/28	[72]
$Cu_{0.25}Ni_{0.5}Zn_{0.25}Fe_2O_4$	ethanol	room temperature	500		75%	18/20	[72]

Note: V_a and V_g represent the sensor voltages in the air and test gas, respectively.

Table 5 Comparison of the morphology and gas sensing performance of various sensors based $ZnFe_2O_4$ composites

Materials	Micro-morphology	Target gas	Operating temperature (°C)	Conc. (ppm)	Response ($S=R_a/R_g$)	$\tau_{res.}/\tau_{rec.}$ (s)	Ref.
$ZnFe_2O_4$/ZnO	nanoparticles decorated nanorod	n-butyl alcohol	260	50	13.6	12/11	[78]
ZnO/$ZnFe_2O_4$	nanoforest	ethanol	275	100	~10.8	~11/5	[79]
ZnO/$ZnFe_2O_4$	flower	acetone	250	50	~8.3	~2/25	[80]
ZnO/$ZnFe_2O_4$	hollow sphere	acetone	280	50	5.2	7.1/10.8	[84]
ZnO/$ZnFe_2O_4$	nanocage	acetone	290	100	25.8	8/32	[85]
ZnO/$ZnFe_2O_4$	Triple shell hollow sphere	acetone	140	20	~5.9	~5.2/12.8	[86]
RGO/$ZnFe_2O_4$	—	acetone	275	10	4.0	4.13/17.6	[96]
ZnO/$ZnFe_2O_4$	hollow tube	acetone	250	5	7.5	336/360	[99]
$ZnFe_2O_4$/α-Fe_2O_3	porous micro-rod	triethyl-amine	305	100	~42.4	~16/26	[100]